Evaluating the chemical levels in soil, groundwater, bay water, bay sediment, and oyster tissue in the Port Bay region

Final Report

Publication CBBEP – 180
Project Number – 2332
February 2024

Prepared by: Kaijun Lu[1], Jack Lloyd[1], Jianhong Xue[1], Jace Tunnell[2], Kristin Nielsen[1], Zhanfei Liu[1]

[1]Marine Science Institute, The University of Texas at Austin, Port Aransas, Texas 78373

[2]Harte Research Institute, Texas A&M University-Corpus Christi, Corpus Chrisi, Texas 78412

Phone: (361) 749-6772
E-mail: zhanfei.liu@utexas.edu

Submitted to:
Coastal Bend Bays & Estuaries Program
1305 N Shoreline Blvd, Suite 205
Corpus Christi, TX 78401

Table of Contents

Executive Summary *3*

1. Introduction *4*

2. Materials and Methods *6*

2.1 Sampling Sites **6**

2.1.1 Terrestrial sampling sites for soil and groundwater 6

2.1.2 Sampling sites for bay water and surface sediment 6

2.1.3 Sampling sites for oyster 7

2.2. Analytical Method **7**

2.2.1 TPH extraction and analysis 7

2.2.2 Pigment extraction and analysis 9

2.2.3 Total suspended solids analysis 10

2.2.4 Nutrients analysis 10

2.2.5 As, Cr, Hg, U, and Ra-226 analyses 10

2.3. Statistical Analysis **11**

3. Results and Discussion *12*

3.1. Hg, U, and Ra-226 in groundwater **12**

3.2. Hg, As and Cr results in bay water **13**

3.3. Hg results in oyster tissue **13**

3.4. Nutrient results in bay water **14**

3.5. Pigment results in bay water **16**

3.6. TPH results in terrestrial soils **17**

3.7. TPH results in bay sediment and water **19**

4. Conclusions *21*

Figures *26*

Tables *36*

Executive Summary

In this project, levels of various chemicals were investigated, including nutrients (NH_4^+, NO_2^- +NO_3^-, and PO_4^{3-}), pigments (chloropigments and carotenoids), total suspended solids, mercury (Hg), uranium (U), radium-226 (Ra-226), as well as polycyclic aromatic hydrocarbons (PAHs) in samples collected near the Port Bay tailings ponds and in the Port Bay. Results indicate that the concentrations of various contaminants, including Hg, U, Ra-226, arsenic (As), chromium (Cr), and PAHs in the soils, groundwater, bay water, bay sediments, and oyster tissues are generally lower than the corresponding critical thresholds, suggesting an acceptable quality of the environment. However, certain sampling sites in close proximity to the tailing ponds and/or the TX-188 highway exhibited relatively higher levels of contamination compared to other locations, indicating a potential impact on the ecosystem. In addition, various chemicals were significantly higher in the water column in Port Bay compared to the adjacent larger bays, revealing the uniqueness of this small shallow system. Specifically, resuspension of bay sediment may have significantly influenced the levels of nutrients, pigments, and PAHs in the water column. PAHs, in particular, can be remobilized from sediment to the water column during wind-driven resuspension events likely due to their preferential association with fine clay minerals. Therefore, while the overall contamination levels may not raise specific concerns, the temporary relocation or elevation of contaminants through resuspension processes may introduce complexities and unforeseen effects on this shallow ecosystem. This underscores the necessity for further investigation and continuous monitoring.

1. Introduction

In January 2022, concerns arose among the community in Aransas County regarding potential contamination from the Sherwin Alumina storage ponds, commonly referred to as tailings ponds, and their impact on Port Bay, an adjacent shallow water system. These concerns were fueled by a widely circulated YouTube video released in December 2021 (www.youtube.com/watch?v=H72F-TnDKps), which suggested that the powerful winds and storm surge associated with Hurricane Harvey in 2017 might have caused contaminants from the tailings ponds to enter the bay, thereby posing potential risks to both the ecosystems and human health of the region.

Of the various pollutants released during aluminum production from bauxite, Mercury (Hg) is particularly pertinent in the context of risk assessment (Donoghue et al., 2014; Oral et al., 2019). Additionally, radionuclides such as Uranium (U) and Radium (Ra), which can be derived from bauxite (Oral et al., 2019), also present significant concerns. The characterization of these chemicals can provide useful information as to whether the Port Bay region is of environmental concern, and whether the source of contamination may be from bauxite residues. Notably, a groundwater characterization study performed by Golder Associates Inc. in 2018 found that U and Ra exceeded action levels in groundwater adjacent to the ponds. Consequently, monitoring the presence of these substances in Port Bay can serve as an indicator of bauxite contamination originating from the nearby tailings ponds, necessitating a comprehensive reevaluation of the environmental impact.

Aside from radioactive nuclides, the generation of total petroleum hydrocarbons (TPHs), polycyclic aromatic hydrocarbons (PAHs) in particular, can also occur at different stages of aluminum production. For instance, the Hall-Héroult process could lead to production of PAHs from the carbon anodes used in the electrolysis cells (e.g., Kvande and Drabløs, 2014; Mercier et al., 2011). PAHs may also be sourced from biomass and gasoline combustion or directly from petroleum contamination (Wang et al., 2014). PAHs are mutagenic and carcinogenic, and can bioaccumulate in food chains, thus eventually impacting human health (Eisler, 1987; Kennish, 2002). Monitoring the concentrations of PAHs near the Port Bay regions (e.g., in nearby soil and in the bay) will provide information on the potential effect of bauxite contamination from the tailings ponds and/or other sources of contamination.

While the production and treatment history of the ponds is relatively unknown to the public, qualitative evidence from Google Earth satellite images has revealed observable changes in the coloration of the ponds over time, primarily attributed to the presence of bauxite. Severe weather events can cause seepage, runoff, and complete failure of tailings ponds; thus the 2017 Hurricane Harvey may have been a major catalyst for the dramatic change in color observed in the ponds pre- and post-hurricane, likely due to the strong wind and storm surge. Combined with the proximity of the ponds to Port Bay, the hydrology of the area, and the intensity of the storm surge and winds, the potential of the contaminated environmental media to be leached and percolated from the tailings ponds into nearby waters, soils and sediments has raised serious concerns. Alternatively, chemicals from the tailings ponds may also infiltrate Port Bay through aquifers and groundwater discharge pathways, which are known mechanisms for transporting freshwater and associated contaminants to coastal areas (Moore, 1996).

The historical data regarding contaminants in Port Bay is limited, with only sporadic water quality data collected by the Texas Commission on Environmental Quality (TCEQ) at the TX-188 bridge, without corresponding sediment data. To the best of our knowledge, there is no other data available for water or sediment in Port Bay to inform conclusions about the potential risk. Therefore, the primary goal of this project was to evaluate the potential contamination from the tailings ponds to the adjacent groundwater, soil, and bay system. Specifically, we measured the levels of Hg, U, Ra and TPHs, in groundwater and soil samples from 5 locations near the tailings ponds. We also evaluated the levels of nutrients, pigments, contaminants (Hg, As, and Cr) in Port Bay water, Hg in oysters collected from the bay, as well as PAHs in water column and surface sediment from up to 8 different sites in the bay spanning 3 different seasons over one year.

2. Materials and Methods

2.1 Sampling Sites

2.1.1 Terrestrial sampling sites for soil and groundwater

Terrestrial soil samples and groundwater samples were collected at 5 sites near Port Bay (Figure 1) in November and December of 2022 (Figure 1). Specifically, Sites A (N28°0'49.6", W97°10'32.2") and B (N28°0'54.7", W97°12'9.7"), situated on the roadside in close proximity to the ponds, were visited on November 10, 2022, while Sites C (N28°0'16.1", W97°9'41.4"), D (N27°58'43.4", W97°10'60"), and E (N28°2'52.9", W97°9'29.5"), located along the coastal line of Port Bay, were sampled on December 6, 2022.

At each site, surface (ca. 5 cm) and deep (ca. 1 m deep) soil samples were collected using an auger (AMS Signature Series Soil Augers, Fondriest), placed in zip-loc bags, and transferred into a -20 °C freezer once returned to the lab within the same day. Depending on the specific sampling site, the waiting time for groundwater to partially fill the drilled hole varied from ca. 10 min to over 1 hr. Once the drilled holes were filled with water, triplicate samples of ca. 1.5 L groundwater were drawn using a pre-rinsed syringe into the bottles with preservatives, which were provided and prepared by PACE Analytical (Mount Juliet lab), a NELAP-accredited lab. Soil samples were used for total petroleum hydrocarbon (TPH) analysis at UTMSI. Groundwater samples were sent to PACE Analytical (Mount Juliet lab) for concentrations of mercury (Hg), and activity levels of Uranium (U) and Radium-226 (Ra-226), within 7 d after collection. Prior to TPH analysis, a fraction of soil samples (ca. 10 g) was freeze-dried for at least 48 hr to remove residual water.

2.1.2 Sampling sites for bay water and surface sediment

Samples of surface water and surface sediment were collected from 8 different sites in Port Bay in December of 2022, May of 2023, and November of 2023 (Figure 1). Specifically, Sites 1 (N27°58'30.1", W97°10'54.4"), 2 (N27°59'14.1", W97°10'24.6"), and 3 (N27°59'47.8", W97°10'12.1") are in the southern part of the shallow bay, while sites 4 (N28°0'11", W97°9'11.1"), 5 (N28°1'20.3", W97°8'53.1"), 6 (N28°2'14.1", W97°8'23.5"), 7 (N28°3'2.3", W97°8'49.7"), and 8 (N28°3'0.9", W97°10'27.7") are in the northern bay, with site 7 at the connection between Copano Bay and Port Bay, and site 8 in the Swan Lake.

At each site, surface water samples (ca. 20 cm) and surface sediment samples (ca. 5 cm) were collected. Water samples were collected with either plastic bottles provided by PACE Analytical or pre-rinsed 4 L amber glass jars depending on the need of analyzing specific parameters. Duplicate sediment samples were collected using a lab-designed coring system and placed in zip-loc bags on ice. Water samples collected with PACE bottles were transferred to a 4 °C fridge and were sent to PACE within 7 d after collection for analyses of mercury (Hg), arsenic (As), and chromium (Cr). Water samples collected with amber jars were separated into different aliquots. One aliquot (ca. 1 L) was filtered through pre-combusted 0.7 μm GF/F filters for total suspended solids (TSS) and pigment analyses, and preserved at -20 °C for subsequent nutrient analyses. The other aliquot of surface water (2 – 3 L) was acidified with 12 N HCl to a final pH of 2, and was extracted for TPH via solid phase extraction.

2.1.3 Sampling sites for oyster

Oyster samples were collected from wild reefs at sites 3, 4, 7 and 8 (Figure 1) during the May 2023 sampling trip. These sites were selected based on both the oyster availability (sites 7 and 8 are close to the oyster farm, and oysters were spotted near site 3) and spatial coverage of sampling area. Oysters were found within the area where water and sediment samples were collected. Four live oysters were collected from each site. Collected oysters were shucked, weighted, and preserved at -80 °C before being sent to PACE Analytical (Green Bay lab) for the analysis of Hg in oyster tissue.

2.2. Analytical Method

2.2.1 TPH extraction and analysis

To better quantify the levels of anthropogenic pollution, the analysis of TPH was focused on polyaromatic hydrocarbons (PAHs), as *n*-alkanes detected in samples from nearby regions are mainly from biogenic sources. Sixteen priority PAHs listed by the US Environmental Protection Agency (EPA) were analyzed: naphthalene (Nap), acenaphthylene (Acy), acenaphthene (Ace), fluorene (Fl), phenanthrene (Phe), anthracene (Ant), fluoranthene (Flu), pyrene (Pyr), benz[a]anthracene (BaA), chrysene (Chr), benzo[b]fluoranthene (BbF), benzo[k]fluoranthene (BkF), benzo[a]pyrene (BaP), indeno[1,2,3-cd]pyrene (InP), dibenz[a,h]anthracene (DBA), and benzo[ghi]perylene (BgP). The standard curve was made

with the standard mixture of 16 US EPA-priority PAHs (AccuStandard), spiked with the deuterated Phe (Phe-d_{10}) as the surrogate standard.

PAHs in water samples were extracted according to the technical note by Biotage (http://www.jysco.com/archives/Biotage/ISOLUTE_TPH_appNote.pdf). Briefly, unfiltered water was acidified with 12 N HCl to a final pH of 2. Forty mL of methanol was added to each sample. Solid phase extraction (SPE) was then used to extract the hydrocarbons from each sample using Isolute TPH columns (Biotage). Prior to the extraction, columns were primed with 150 mL of methanol and 100 mL of acidified LC/MS grade H_2O (pH of 2). Samples were then extracted at a flow rate of 30 mL/min. After ca. 80% of the solution had been extracted, 100 mL of acetone and 200 mL of pH ~2 H_2O were added to each sample before continuing with the extraction. This step of rinsing is crucial in making sure all possible hydrocarbons were extracted. The compounds adsorbed to the solid phase were then eluted with four rounds of 5 mL of hexane per cartridge. The eluted solution was concentrated to 5 mL via blowing with N_2 gas, and stored in a freezer until further analysis.

Extraction of PAHs and alkanes from soil and sediment samples was modified after Wang et al. (2012). Briefly, ca. 5 g of freeze-dried soil or sediment samples were extracted with an accelerated solvent extraction system (ASE300, DIONEX, USA) using a mixture of acetone and dichloromethane (2000 mL; 1:1 v/v). Deuterated hexadecane (Hex-d_{34}) and phenanthrene (Phe-d_{10}) were spiked into each sample as surrogate standards to calculate the recovery rates. The extraction cells were heated to 100 °C until the pressure of 10 MPa was reached. The static time was 5 min, with a flush volume of 60%, and a purge time of 90 s. The final volume of the extract was approximately 30 – 40 mL and was further concentrated with methylene chloride (DCM) to 2 mL by gently blowing the samples with N_2 gas.

PAHs were analyzed using gas chromatography coupled with a mass spectrometer (GC-MS; Shimadzu, GCMS-QP2020). A siloxane-based column (SH-Rxi-5Sil; 30 m × 0.25 mm i.d., film thickness 0.25 μm) was used. The 16 priority PAHs listed by the US EPA were measured under selective ion monitoring mode (SIM). Helium (He) was used as carrier gas at a flow rate of 2 mL/min, and a split ratio of 10 under linear velocity mode. The oven temperature was held at 40 °C for 1 min, increased to 240 °C at a rate of 10 °C/min, then increased to 280 °C at a rate of 4 °C/min and held for 10 min, and finally increased to 320 °C

at a rate of 10 °C/min and held for 5 min. The injection and ion source temperatures are set to be 250 °C and 260 °C, respectively. The injection volume was 1 μL.

The *n*-alkanes (C_8 – C_{39}) were analyzed according to the methods of Bacosa et al (2021). Briefly, *n*-alkanes were analyzed by the same GC-MS and the same column as described in the PAH analysis above. The oven temperature was held at 50 °C for 1 min, increased to 280 °C at a rate of 8 °C/min and held for 36 min, and increased to 0 °C at 10 °C/min. *n*-Alkanes were quantified based on surrogate standard Hex-d_{34} and mixture of *n*-alkane external standards (C_8 – C_{39}).

For quality assurance/quality control (QA/QC), method blanks were analyzed by the same procedure as the samples to determine any background contamination. None of the 16 PAHs or *n*-alkanes were detected. The average recovery rate was 103 ± 19% for PAHs (n = 40) and 111 ± 42% (n = 36) for *n*-alkanes, based on spiked surrogate standards (Phe-d_{10} and Hex-d_{34}).

2.2.2 Pigment extraction and analysis

Pigment extraction and analysis were performed with the GF/F filters. The method followed Sun et al. (1991) with slight modifications (Liu and Xue, 2020). Briefly, the filter was extracted twice with 100% acetone by sonication, then combined and analyzed using high performance liquid chromatography (HPLC) coupled with UV–vis and fluorescence detectors. Tetrabutylammonium acetate in methanol (eluent A) and methanol (eluent B) were used as eluents. Chl a and phaeopigments were detected by fluorescence (Ex: 440 nm; Em: 660 nm), and carotenoids by UV–vis absorbance (450 nm). The detected pigments included chlorophyll a, chlorophyll b, chlorophyll c2, fucoxanthin, 19-hex-fucoxanthin, 19-but-fucoxanthin, zeaxanthin, alloxanthin, peridinin, prasinoxanthin, and lutein. Lutein eluted separately from zeaxanthin and was generally 15-20% of the zeaxanthin concentration. The concentrations of pigments were determined by comparison of peak retention time to certified standards (DHI, Denmark), and relative Chl a contributions of major phytoplankton taxa calculated following Reyna et al. (2017) and Qian et al. (2003).

2.2.3 Total suspended solids analysis

Samples for the analysis of total suspended solids (TSS) were collected during the November 2023 trip, and were measured following the U.S. Environmental Protection Agency (EPA) method 160.2 (https://19january2017snapshot.epa.gov/sites/production/files/2015-06/documents/160_2.pdf). Briefly, the pre-combusted 47 mm 0.7 µm GF/F filters were dried and weighted prior to filtration. Two hundred mL of surface water was filtered for each filter. The filters were then dried in an oven at 103 °C until constant weights were reached (for at least one hour; weight loss is less than 0.5 mg).

2.2.4 Nutrients analysis

Nitrate (NO_3^-) and nitrite (NO_2^-), ammonium (NH_4^+), and phosphate (PO_4^{3-}) concentrations were determined using a Lachat nutrient auto-analyzer using the standard colorimetric methods.

2.2.5 As, Cr, Hg, U, and Ra-226 analyses

Groundwater samples (collected in December 2022) were submitted to PACE lab (Mount Juliet lab) to analyze mercury (Hg), Uranium (U), and Radium-226 (Ra-226). The EPA method 7470A was used for Hg analysis (https://www.epa.gov/sites/default/files/2015-07/documents/epa-7470a.pdf). The EPA method D5174 was used for U analysis (https://www.epa.gov/dwanalyticalmethods/approved-drinking-water-analytical-methods), and the Standard Method 7500-Ra B (https://www.nemi.gov/methods/method_summary/7616/) was used for Ra-226 analysis. Detection limit is 0.0001 mg/L for Hg analysis, 0.001 mg/L for U, and less than 0.09 pCi/L for Ra-226.

In addition, surface water samples were submitted to PACE lab to analyze Hg (December 2022; PACE Mount Juliet lab), arsenic (As; November 2023; PACE Allen lab) and chromium (Cr; November 2023; PACE Allen lab). Hg was measured using the mentioned EPA 7470A method, while As and Cr were measured using EPA method 200.7 (https://www.epa.gov/esam/method-2007-determination-metals-and-trace-elements-water-

and-wastes-inductively-coupled). The method detection limit is 0.0001 mg/L for Hg, 0.004 mg/L for As and 0.0007 mg/L for Cr.

Hg in oyster tissue were submitted to PACE lab (Green Bay lab). The analytical method is EPA 245.6 (https://cfpub.epa.gov/si/si_public_record_Report.cfm?Lab=NERL&dirEntryId=46104). The method detection limit is 0.019 mg/kg.

2.3. Statistical Analysis

Statistical analyses, including t test and analysis of variance (ANOVA), were conducted in Excel. Principal component analysis (PCA), which is a multivariate regression analysis examining compositional differences among samples, was conducted using R (version 4.2.3). Concentrations of each parameter were standardized by subtracting the means and dividing by the standard deviations before PCA.

3. Results and Discussion

3.1. Hg, U, and Ra-226 in groundwater

Concentrations of Hg in the groundwater were below detection limit (< 0.0001 mg/L) at all 5 sites (Table 1). U concentrations ranged from below detection limit (< 0.001 mg/L) at Site D to ca. 0.039 mg/L at Site B, and were significantly different among the sites (ANOVA; $p = 0.02$). Subsequent t-test further confirmed that the U concentration at Site B was significantly higher than that at Site D ($p = 0.04$) and Site E ($p = 0.05$), and U concentration at Site C was significantly higher than that at Site D ($p = 0.01$).

Similar to U, the highest level of Ra-226 was found at Site B, with a range from 1.19 pCi/L at Sites C and E to 2.06 pCi/L at Site B. However, there were no differences in Ra-226 level among the 5 sites (ANOVA, $p = 0.80$).

The U concentrations measured at the 5 sites were lower than the EPA's Maximum Contaminant Level (MCL) of 0.03 mg/L for drinking water, except for Site B at a concentration of 0.039 mg/L. However, it should be noted that the EPA MCL standard applies specifically to drinking water and not necessarily to groundwater. The Ra-226 levels at all sampling sites were below EPA's MCL of 5 pCi/L.

Uranium (U) is a naturally occurring radioactive element that existed when the Earth was born, or primordial. The Ra-226 is one element in the U-238 decay series, a decay product directly from thorium-230 (Th-230) and has a half-life of 1600 years. U and Ra-226 exist naturally and are soluble, but their concentrations in groundwater may depend on the types or ages of specific minerals. The U and Ra-226 measured from the groundwater at the five sampling sites were below the EPA MCL for drinking water. This result indicates that the groundwater quality is within acceptable limits in the aspect of these two chemicals.

To compare with published results, the Ra-226 levels measured in this work are within the reported range (1.2 - 11.4 pCi/L) in drinking water from five aquifers (Hickory, Gulf Coast, Dockum, Edwards-Trinity and Ogallala aquifers) in Texas (Landsberger and George, 2013), as well as in other regions (e.g., 0.05 - 13.3 pCi/L in Brazil, Almeida et al., 2004; generally 1 - 5 pCi/L in US, Michel and Jordana, 1987). In addition, the Ra-226 levels from this work agree with the 2019 Preliminary Groundwater Assessment Report (0 - 3.1 pCi/L) near the Port Bay region (Texas Commission on Environmental Quality, 2019). Concentrations of U from this work (< 0.001 - 0.039 mg/L) agree with the reported values in

water wells of the Edwards-Trinity aquifer in Texas (< 0.001 - 0.154 mg/L, Hudak, 2018), as well as in the High Plains (HP) and Central Valley (CV) aquifers of US (mean concentration of ca. 0.01 mg/L, Nolan and Weber, 2015). The 2019 Preliminary Groundwater Assessment Report reported a U level of 0.0033 - 0.27 mg/L, with most sampled wells exceeding the MCL (Texas Commission on Environmental Quality, 2019). The results from this work are at the lower end of the range. However, the U concentration at Site B was slightly higher than the MCL threshold of 0.03 mg/L, which warrants further attention.

3.2. Hg, As and Cr results in bay water

Hg, As, and Cr were barely detectable in surface water of the Port Bay. Only Site 3 had a detectable As concentration of 0.008 mg/L, which is below the drinking water threshold (0.01 mg/L) established by EPA. Similarly to the case of U, the EPA limit is more focused on drinking water, and may not necessarily be applied to bay water.

3.3.Hg results in oyster tissue

Concentrations of Hg in oyster tissue (wet weight) ranged from 0.007 mg/kg (Site 7) to 0.021 mg/kg (Site 3; Table 1). The fact that Hg in bay water is below detection limit, yet Hg is detected in the tissue of oysters may result from the bio-accumulative nature of Hg. Risks of Hg to ecological and human health are estimated using Hazard Quotients (HQ):

$$Hazard\ Quotients = \frac{[Hg]\ measured\ at\ site}{Screening\ Value}$$

These are generated using a generic formula that compares the concentration of the contaminant measured in water, sediment, or biota (oysters) to a screening value that is determined by regulatory agencies. Screening values will differ according to whether the risk assessor is evaluating contaminated sediment, soil, water, air or tissues and will also be different depending on whether the evaluation is for animals or humans. An HQ greater than 1 indicates that the concentration of the contaminant at the site is above the screening value and may pose a risk to animals or humans. When the HQ is less than 1, it indicates that the risk is low or negligible. The US EPA does not have specific screening values for Hg in tissues (only in sediment and water). However, the European Union has screening value

known as Environmental Quality Standards (ESQs; 0.02 mg/kg, wet weight; Table 1), which could be used for comparison.

In risk assessments, when there are less than 10 measurements to use in the analysis, it is standard practice to use the maximum measured concentration at each site (denoted as HQ Max in Table 1). The average concentrations for each site were also evaluated (denoted as HQ Average in Table 1). The EQS Biota value is a non-specific screening value that could apply to the tissues of any aquatic organism. If any species has tissue concentrations over 0.02 mg/kg WW of mercury, its health should be protected. Using EQS Biota, it was found that only Site 3 had one replicate with levels of mercury in oysters high enough to yield a HQ Max greater than 1. However, it should also be noted that none of the average concentrations exceeded the screening value (i.e., all HQ Average less than 1).

It remains unclear why oysters from Site 3 possessed a relatively higher Hg in their tissues (Single factor ANOVA, $p = 0.0002$), even though the averaged values are below the threshold. It is possible that the location of Site 3, which is near the bridge (highway TX-188) with heavy traffic, may contribute to the observed high concentrations.

3.4.Nutrient results in bay water

Nutrients in Port Bay surface water showed statistically significant differences between different sampling dates (Table 3). Compared with samples collected in December 2022, NH_4^+ concentration in May 2023 was significantly lower (paired t-test, $p = 0.005$), while concentration of NO_x (NO_2^- and NO_3^-) was significantly higher ($p = 0.000004$), as no NO_x was measured in December 2022. Concentrations of phosphate (PO_4^{3-}) were more complicated and were location specific: the north bay showed significantly lower concentrations of PO_4^{3-} in May 2023 ($p = 0.000001$), though the difference with south bay was insignificant ($p = 0.07$; i.e., concentrations were considered to be the same statistically).

The observed differences in nutrient concentrations can be attributed, in part, to the different weather conditions and the extreme shallowness of the bay. Based on field measurements, the shallowest regions of Port Bay (e.g., sites 1 – 3 and 8) have a depth of about 1 – 2 feet, while the deepest site (Site 7, connected to Port Bay) is approximately 3 – 4 feet deep. Samples were collected during windy weather in December 2022, when the resuspension of sediment was quite strong, particularly in the north region of the bay. On the

other hand, the weather was calm in May 2023. As the major removal process of PO_4^{3-} from the water column is through the burial process in sediment, the resuspension of sediment would lead to the re-release of PO_4^{3-} and thus result in much higher concentrations.

The difference in NO_x supports this speculation. The relatively high NO_x concentrations (average of 34 μmol N/L) in May 2023 and the non-detectable levels of NO_x in December 2022 suggest the existence of a strong N-removal process in Port Bay, such as denitrification and anaerobic ammonium oxidation (anammox), particularly during windy conditions. Previous studies have shown that the turbulent energy accelerates the sediment denitrification processes (i.e., the transformation of nitrate to nitrogen gas) in shallow aquatic systems (Hurst et al., 2019; Zhu et al., 2021). Even though denitrification is an anaerobic process, the resuspension of sediment likely facilitates increased interaction between nitrate and denitrifying microbes, and thus could lead to very fast rates of nitrate reduction (Hurst et al., 2019). Under calm conditions, diffusion might limit nitrate flux into sediment, and denitrification is thus limited by the availability of substrate.

Due to logistics issues, not all sites were visited in November 2023, but nutrient concentrations at the visited sites fell between those of December 2022 and May 2023. The PO_4^{3-} concentrations (from below detection limit to the highest of 140 ppb at Site 3; Table 3) resembled those in May 2023 (i.e., relatively low except for a few sites), while NO_x concentrations were similar to those in December 2022 (i.e., almost undetectable; Table 3). Weather conditions on the sampling date (November 17th, 2023) were rather calm (highest wind speed about 9 km/h), which offered an explanation to the observed low concentrations of PO_4^{3-}. On the other hand, strong winds were recorded in the days prior to the November sampling trip (wind speed over 25 km/h 3 days before sampling trip). Given an average denitrification rate on the level of nmol/(L·d), the removal of nitrate from the system would require several days, explaining why the concentrations of NO_x were also low. The results of total suspended solids (TSS) analysis also supported this speculation, as TSS ranged from 63 – 104 mg/L during the sampling time (Table 4), falling into a typical range for marine systems (consistent with previous UT technical report, 2011) and much higher than previously reported values in seagrass beds (average of 13 mg/L; e.g., Cuddy, 2015)

Overall, the shallowness of the bay, together with the resuspension of bay sediment, which is readily affected by weather conditions, plays an important role in determining nutrient concentrations in Port Bay.

3.5.Pigment results in bay water

Using pigments as biomarkers to assess phytoplankton community is an effective approach for surveying a large quantity of samples over wide spatial and temporal scales, and for evaluating the ecosystem health. As expected, chlorophyll a (Chl a) was the dominant pigment in all sites during both sampling events, ranging from ca. 1700 to ca. 6700 ng/L in December 2022, and from ca. 1500 to ca. 7800 ng/L in May 2023. The highest Chl a concentrations were found at Site 1 in December 2022, and at Site 2 in May 2023 (Table 5). Overall, concentrations of Chl a at sites in the south region (i.e., sites 1, 2, and 3) of the bay were higher than those in the north region, even though the difference was only significant in May 2023 (p = 0.06 in December 2022; p = 0.001 in May 2023). For comparison, during wet periods, Chl a in Copano Bay averages about 7000 ng/L, Aransas Bay about 5300 ng/L, and Ship channel about 3700 ng/L (Douglas et al., 2023). The relatively low Chl a concentrations, particularly in the north region, may also be attributed to the shallowness of Port Bay, i.e., high turbidity that may have limited light penetration and thus the algal growth. On the other hand, the south bay could experience higher nutrient inputs from the surrounding watershed and vegetation (also indicated by the difference in the watercolors).

The composition of carotenoids, including peridinin, 19-but-fucoxanthin, fucoxanthin, prasinoxanthin, 19-hex-fucoxanthin, diadinoxanthin, alloxanthin, zeaxanthin, lutein, changed significantly from December 2022 to May 2023 (Figure 2). In December 2022, carotenoids were dominated by fucoxanthin, followed by alloxanthin and zeaxanthin, indicating the dominance of diatoms, followed by cryptophytes and cyanobacteria in the phytoplankton community (Liu and Xue, 2020). In May 2023, zeaxanthin was the sole dominant carotenoid. Since cyanobacteria could be a major contributor of zeaxanthin, the dominance of zeaxanthin in May 2023 indicated the proliferation of cyanobacteria in Port Bay. Combined with the nutrient data (section 3.4), calm water column conditions may be particularly important for cyanobacterial growth in this shallow bay.

3.6. TPH results in terrestrial soils

Concentrations of PAHs in terrestrial surface soils ranged from 73.6 ng/g dried soil at Site A to 140.6 ng/g at Site D. Concentrations of PAHs in deep soil (ca. 1 m deep) were generally higher than those in surface soil, ranging from 77.5 ppb at Site D to 148.5 ppb at Site B (Table 6; Figure 3). There was no difference among all surface soil samples (ANOVA, $p = 0.1$). However, the PAH concentration in the deep soil was lower at Site C than those at Site B ($p = 0.03$) and Site D ($p = 0.04$).

PAHs are often grouped according to their molecular weights or number of aromatic rings, those with 2 or 3 rings are grouped as low molecular weight (LMW) and those with 4 or more rings are grouped as high molecular weight (HMW) ones. PAHs in the soil samples were dominated by LMW PAHs, particularly phenanthrene and anthracene, accounting for ca. 65 – 100% of total PAHs. In contrast, HMW only constituted a minor fraction of total PAHs (0 – 35%). Fluoranthene and pyrene were the only detectable HMW PAHs in the soil samples.

The concentrations of *n*-alkanes in surface soil ranged from 4184.8 ppb at Site B to 5981.2 ppb at Site D. Similar to PAHs, concentrations of *n*-alkanes were higher in deep soil than those in surface, ranging from 4562.3 ppb at Site C to 8145.1 ppb at Site E (Table 7; Figure 4). *n*-Alkanes were dominated by the ones with a carbon number ranging from 21 to 29.

TPHs, particularly PAHs, in the solid phase of the aquifer at the 5 terrestrial soil sites were found to be on the same order of magnitude as what were previously measured from other local bays, such as Corpus Christi, Mission-Aransas, and Matagorda bays (~10^2 ppb; unpublished data in Liu Lab; Liu et al., 2011). PAHs concentrations at the study sites were also comparable to those measured in the surface sediments from Gulf of Mexico (e.g., Wade et al., 2008). The reported concentrations in this study were also in the range, even though at the lower end, of soils collected over a much larger scale. A meta-study showed a range of 4.8 to 186000 ng/g of total PAHs in soils across the globe, with a rough mean of ca. 200 ng/g in the North American prairie regions (Wilcke, 2007). The dominance of naphthalene and phenanthrene in this study (Figure 3) is consistent with the findings of significant contributions of naphthalene and phenanthrene when total PAHs are relatively low (Wilcke, 2007).

In contrast, PAHs from soil samples in this work were roughly an order of magnitude lower than the surface sediment from Galveston Bay (over 2000 ng/g, Santschi et al., 2001), a heavily polluted water body. The nature of the sample (i.e., soil samples vs. sediment samples), as well as sampling locations (i.e., light-traffic roadside vs. highly industrialized seaport), may be the major causes of the observed discrepancies. For example, soil from deeper layers may have less exposure of PAHs deposition from the air, while sediments often receive such pollutants from air deposition through the water column (often in particulate forms), or direct contamination through petroleum or gasoline/diesel combustion due to shipping traffic.

Statistical analyses further revealed the compositional differences among sampling sites. Specifically, principal component analysis (PCA) is often used to distinguish compositional patterns among environment samples when many chemical parameters are available for the samples (e.g., Xue et al., 2011; Yunker et al., 1995). In the present work, PCA was performed based on the PAH composition at different soil sites. With principal component 1 (PC 1) explaining over 43% of the variance, and the other 33% of the variance attributed to PC 2, the 5 soil sites are rather similar in terms of their PAH composition, as the major difference is between surface and deep samples (Figure 5). Higher levels of PAHs, high molecular weight PAHs in particular, may be better preserved in deep soil samples due to either the blockage of sunlight that can photo-transform PAHs, or the abundance of clay minerals that HMW PAHs preferentially adsorb to (e.g., Zhao et al., 2023; Figures 3 and 5). Nevertheless, the similar PAHs concentration and composition among different sampling sites suggest that the influence from the tailings pond on PAHs may be minimal, if any. The lower levels of PAHs at these sites, when compared to adjacent regions, also point to the limited influence of tailings ponds in PAHs.

The composition of PAHs can be used to derive the contamination sources. For instance, the ratios of anthracene (Ant) to anthracene and phenanthrene (Ant + Phe), and fluoranthene (Flu) to fluoranthene and pyrene (Flu + Pyr) can help differentiate the sources of PAHs. An Ant to Ant + Phe ratio greater than 0.1 indicates that PAHs are sourced from incomplete combustion, while ratio smaller than 0.1 suggests sources of petroleum products (e.g., spilled oil; Wang et al., 2012; Yunker et al., 2002). Similarly, whether PAHs are originated from oil source, coal and biomass burning, or incomplete combustion of oil

products can be determined by the Flu to Flu + Pyr ratio, with less than 0.4 indicating an oil source, exceeding 0.5 indicating coal and biomass burning, and between 0.4 and 0.5 indicating incomplete combustion of oil products. The high Ant to Ant + Phe ratios detected at the sampling sites in this work suggest that PAHs were generally from incomplete combustion. Together with the Flu to Flu + Pyr ratio, the results suggest that oil source or incomplete coal and biomass burning potentially may have a major effect on PAHs in the sampled soils (Figure 6), which could be a result of aluminum production from bauxite (e.g., Busetti et al., 2014; Oral et al., 2019), but could also originate from normal activities (e.g., cars, boats, etc.). Therefore, the composition of PAHs in the sampling soil sites did not provide a decisive linkage to the tailings ponds.

3.7. TPH results in bay sediment and water

Concentrations of PAHs in surface sediment of Port Bay ranged from 93.1 ng/g dried sediment at Site 2 to over 377 ng/g at Site 3 (Table 8; Figure 7). On the other hand, concentrations of PAHs in surface water ranged from 11.3 ppb at Site 7 to 21.2 ppb at Site 2 (Table 9; Figure 8).

Even though total concentration of PAHs in sediments of Port Bay were higher than those from terrestrial soil sites (Tables 6 and 7), in terms of total concentrations, it was on the similar level as those measured values from other local bays, such as Corpus Christi, Mission-Aransas, and Matagorda bays (unpublished data; Liu et al., 2011), and was lower than the TCEQ established action level (https://www.tceq.texas.gov/downloads/remediation/pst/responsible-party/actionlevels.pdf). The highest concentration was found at Site 3 (377 ng/g), followed by a total concentration of 296 ng/g at Site 8. It was indeed not surprising to see that Site 3 had the highest PAHs in sediment, given that this site also had the highest As level, as well as the highest Hg in oyster (sections 3.2 and 3.3). As previously mentioned, the exact reason for the abnormal chemical parameters measured at Site 3 remained unclear. However, results from multiple angles (e.g., As concentration in bay water, Hg concentration in oyster tissue; sections 3.2 and 3.3) suggested that the highway (TX-188) through traffic contamination might play an important role. For example, the runoff water from the highway could result in elevated concentrations of various chemicals, PAHs in particular.

Unlike the total concentration, there is a drastic difference between the composition of PAHs in Port Bay sediments and those in other bays. Anthracene was the dominant PAH, ranging from 20.4 ng/g in Site 2 to 131.9 ng/g in Site 3, followed by phenanthrene, fluoranthene, and pyrene. LMW fractions dominated PAHs in Port Bay sediment, accounting for 50 – 79% of total PAHs. On the other hand, fluoranthene and pyrene were the only detectable HMW PAHs. Other 5 – 6 ring PAHs (e.g., benzo[b]fluoranthene, benzo[k]fluoranthene, benzo[a]pyrene, and indeno[1,2,3-cd]pyrene) were all below detection limit in Port Bay sediment. HMW PAHs generally have a higher proportion than LMW PAHs, due to their higher hydrophobicity. Specifically, HMW PAHs represent up to 80% of total concentrations in the sediments of Corpus Christi Bay and Mission-Aransas Estuaries (unpublished data), with 5 – 6 ring PAHs representing over 70% of total PAHs. The observed low proportion of HMW PAHs suggests an additional removal process of HMW PAHs in the Port Bay region.

Using the same Ant/(Ant + Phe) and Flu/(Flu + Pyr) ratio, it is clear that the incomplete combustion of coal and biomass was the major source of PAHs in Port Bay sediment (Figure 9). As previously mentioned, aluminum production from bauxite (e.g., Busetti et al., 2014; Oral et al., 2019) can generate PAHs matching this signature, but possible contributions from normal activities (such as cars, boats activities) cannot be ruled out. Therefore, the composition of PAHs in the surface sediment does not provide a decisive linkage to the tailings ponds, either.

PAHs in surface water showed a quite different story. Total concentrations of PAHs in surface water (11.3 – 21.2 ppb; Table 9) were much higher than those in Corpus Christi Bay and Mission-Aransas Estuaries (3.7 – 8.3 ppb; unpublished data). These concentrations were slightly lower than, but were generally on a similar level as, the reported values in industrialized regions (e.g., Kryzevicius et al., 2020; Qiu et al., 2009). Source analysis further revealed that the incomplete combustion of oil products was the major source (Figure 10). This was of particular interest, given the size and the location of Port Bay, as well as its much lighter ship traffic.

In addition, HMW PAHs consist of 86 – 95% of total PAHs (Figure 8). This fraction is also higher than the averaged 85% in Corpus Christi Bay and Mission-Aransas Estuaries, and was in sharp contrast with the compositions in surface sediments. Specifically, the

concentrations of benz[a]anthracene, benzo[b]fluoranthene, benzo[k]fluoranthene, benzo[a]pyrene, indeno[1,2,3-cd]pyrene, and dibenz[a,h]anthracene have exceeded the TCEQ established action level. Together with the low proportion of HMW PAHs in the sediments of Port Bay, such a high fraction of HMW PAHs in water suggests a release of HMW PAHs from the sediment.

Given the shallowness of Port Bay, wind driven resuspension of sediments or other forces play an important role in determining many chemical parameters of the bay, as mentioned for nutrients. Resuspension of sediments also affects the distribution of PAHs. Previous studies have shown that resuspension can lead to an increase in the concentrations of total PAHs (e.g., Bancon-Montigny et al., 2019; Feng et al., 2008, 2007; Latimer et al., 1999; Yang et al., 2008, etc.), with a preferential release of HMW PAHs (Guigue et al., 2017). As previously mentioned, weather conditions in December of 2022 were windy, and the resuspension was strong, which could have possibly led to the remobilization of HMW PAHs from surface sediment to the water column. The HMW PAHs are also less soluble and more hydrophobic, thus maybe preferentially being adsorbed to fine clay minerals (Wang et al., 2016). Strong resuspension due to the shallow water depth in Port Bay, therefore, may lead to high turbidity as evidenced by the high levels of TSS and thus high levels of HMW PAHs. This could also explain the low levels of PAHs in the sediment. This speculation was further supported by the following sampling trip in May 2023, when the total PAHs concentrations in water column under low resuspension condition (or less windy) were extremely low.

4. Conclusions

This study shows that the concentrations of Hg (below detection limit of 0.0001 mg/L), U (< 0.001 - 0.039 mg/L), and Ra-226 (1.19 - 2.06 pCi/L) in the groundwater near Port Bay, As (< 0.004 – 0.008 mg/L), Hg (< 0.0001 mg/L), and Cr (< 0.0007 mg/L) in bay water, as well as Hg in oyster tissue collected in the bay (0.01 – 0.02 mg/kg), were generally lower than the corresponding alert thresholds (e.g., EPA drinking water standards, TCEQ established action level, and European Union Environmental Quality Standards) suggesting an acceptable quality of the environment. However, some sampling sites (either close to the tailings pond or near the highway) did show a higher level of contamination, suggesting the

potential impact could not be excluded. Total concentrations of 16 US EPA PAHs in terrestrial soils near Port Bay were 73.6 – 193.2 ng/g in surface and deep soil samples. This concentration range is significantly lower than regions with high petroleum pollution. While the compositions of PAHs in these terrestrial soils suggest incomplete combustion of coal and biomass may be the major source, the source analysis does not provide a decisive connection to the tailing ponds. Overall, even though the current contaminant levels in the Port Bay region do not pose an immediate threat, further monitoring of the bay is necessary, given its proximity to the tailing ponds, and the development of oyster and shrimp farming in the area.

Work focusing on the nutrients, concentrations of pigment, as well as PAHs in the bay shows that Port Bay indeed is a quite unique system. With an average depth of less than 2 m, the geochemical behaviors of various chemical parameters in Port Bay are strongly affected by its shallowness, and sediment resuspension, as shown by this study. The nutrient regime is mainly determined by resuspension. During strong resuspension, the whole bay is enriched in PO_4^{3-} (22.3 – 82.6 ppb), while depleted in NO_x (undetectable; December 2022) likely due to enhanced denitrification. On the other hand, levels of NO_x are relatively high when the water column is calm (21.7 – 43.3 ppb) but concentrations of PO_4^{3-} are lower (0 – 62.4 ppb). The resuspension may also have complicated effects on phytoplankton compositions, with cyanobacteria being the dominant species during the calm condition. Finally, resuspension greatly affects the total concentrations and compositions of PAHs in the bay. The resuspension of sediment leads to the remobilization of absorbed PAHs, particularly the high molecular weight ones, into the water column. While the total concentrations of PAHs may not surpass the critical threshold, the process of resuspension could potentially lead to a temporary elevation of PAH levels in the water column. This temporary increase may introduce complexities and unforeseen effects on the shallow ecosystem, particularly on filter feeders such as oysters, which would warrant additional attention and investigation.

Acknowledgement

We would like to thank Captain Frank Ernst, Xiangtao Jiang, Maggie Monroe, Kylee Hutchinson, Daniel Fraser, and Clay Addison for their help with sample collection and analysis. We would also like to thank Aransas County, the Aransas County Navigation District, and the Coastal Bend Bays & Estuaries Program for providing funding for this research.

References

Almeida, R.M.R., Lauria, D.C., Ferreira, A.C., Sracek, O., 2004. Groundwater radon, radium and uranium concentrations in Região dos Lagos, Rio de Janeiro State, Brazil. J. Environ. Radioact. 73, 323–334. https://doi.org/10.1016/j.jenvrad.2003.10.006

Bacosa, H.P., Kang, A., Lu, K., Liu, Z., 2021. Initial oil concentration affects hydrocarbon biodegradation rates and bacterial community composition in seawater. Mar. Pollut. Bull. 162, 111867. https://doi.org/10.1016/j.marpolbul.2020.111867

Bancon-Montigny, C., Gonzalez, C., Delpoux, S., Avenzac, M., Spinelli, S., Mhadhbi, T., Mejri, K., Hlaili, A.S., Pringault, O., 2019. Seasonal changes of chemical contamination in coastal waters during sediment resuspension. Chemosphere 235, 651–661. https://doi.org/10.1016/j.chemosphere.2019.06.213

Busetti, F., Berwick, L., McDonald, S., Heitz, A., Joll, C.A., Loh, J., Power, G., 2014. Physicochemical Characterization of Organic Matter in Bayer Liquor. Ind. Eng. Chem. Res. 53, 6544–6553. https://doi.org/10.1021/ie4028268

Cuddy, M., 2015. The Effects of Dissolved Oxygen, pH, and Light on Seagrass Distributions in Corpus Christi Bay and the Mission-Aransas NERR. GIS Water Resour.

Donoghue, A.M., Frisch, N., Olney, D., 2014. Bauxite Mining and Alumina Refining: Process Description and Occupational Health Risks. J. Occup. Environ. Med. 56, S12. https://doi.org/10.1097/JOM.0000000000000001

Douglas, S., Xue, J., Hardison, A., Liu, Z., 2023. Phytoplankton community response to a drought-to-wet climate transition in a subtropical estuary. Limnol. Oceanogr. 68, S187–S201. https://doi.org/10.1002/lno.12348

Eisler, R., 1987. Polycyclic Aromatic Hydrocarbon Hazards to Fish, Wildlife, and Invertebrates: A Synoptic Review. Fish and Wildlife Service, U.S. Department of the Interior.

Feng, J., Shen, Z., Niu, J., Yang, Z., 2008. The role of sediment resuspension duration in release of PAHs. Chin. Sci. Bull. 53, 2777–2782. https://doi.org/10.1007/s11434-008-0389-z

Feng, J., Yang, Z., Niu, J., Shen, Z., 2007. Remobilization of polycyclic aromatic hydrocarbons during the resuspension of Yangtze River sediments using a particle entrainment simulator. Environ. Pollut. 149, 193–200. https://doi.org/10.1016/j.envpol.2007.01.001

Guigue, C., Tedetti, M., Dang, D.H., Mullot, J.-U., Garnier, C., Goutx, M., 2017. Remobilization of polycyclic aromatic hydrocarbons and organic matter in seawater during sediment resuspension experiments from a polluted coastal environment: Insights from Toulon Bay (France). Environ. Pollut. 229, 627–638. https://doi.org/10.1016/j.envpol.2017.06.090

Hudak, P.F., 2018. Associations between Dissolved Uranium, Nitrate, Calcium, Alkalinity, Iron, and Manganese Concentrations in the Edwards-Trinity Plateau Aquifer, Texas, USA. Environ. Process. 5, 441–450. https://doi.org/10.1007/s40710-018-0296-5

Hurst, N.R., White, J.R., Xu, K., Ren, M., 2019. Nitrate reduction rates in sediments experiencing turbulent flow conditions. Ecol. Eng. 128, 33–38. https://doi.org/10.1016/j.ecoleng.2018.12.027

Kennish, M.J., 2002. Environmental threats and environmental future of estuaries. Environ. Conserv. 29, 78–107. https://doi.org/10.1017/S0376892902000061

Kryzevicius, Z., Mickuviene, K., Bucas, M., Vilkiene, M., Zukauskaite, A., 2020. Vertical distribution of polycyclic aromatic hydrocarbons in the brackish sea water column: ex situ experiment. PeerJ 8, e10087. https://doi.org/10.7717/peerj.10087

Kvande, H., Drabløs, P.A., 2014. The Aluminum Smelting Process and Innovative Alternative Technologies. J. Occup. Environ. Med. 56, S23. https://doi.org/10.1097/JOM.0000000000000062
Landsberger, S.G., George, G., 2013. An evaluation of 226Ra and 228Ra in drinking water in several counties in Texas, USA. J. Environ. Radioact., 6th International Symposium on In Situ Nuclear Metrology as a Tool for Radioecology (INSINUME 2012) 125, 2–5. https://doi.org/10.1016/j.jenvrad.2013.02.016
Latimer, J.S., Davis, W.R., Keith, D.J., 1999. Mobilization of PAHs and PCBs from In-Place Contaminated Marine Sediments During Simulated Resuspension Events. Estuar. Coast. Shelf Sci. 49, 577–595. https://doi.org/10.1006/ecss.1999.0516
Liu, Z., Wang, Z., Liu, J., 2011. The distribution of polycyclic aromatic hydrocarbons in surface sediments within the Mission-Aransas National Estuarine Research Reserve, Texas. Mar. Sci. Inst. Univ. Tex.
Liu, Z., Xue, J., 2020. The lability and source of particulate organic matter in the northern Gulf of Mexico hypoxic zone. J. Geophys. Res. Biogeosciences 125, e2020JG005653. https://doi.org/10.1029/2020JG005653
Mercier, G., Blais, J.-F., Dhenain, A., Chartier, M., 2011. Improvement of a three-step process for the treatment of aluminium hazardous wastes containing PAHs (benzo[b,j,k]fluoranthene and chrysene) and fluoride. Environ. Technol. 32, 1883–1893. https://doi.org/10.1080/09593330.2011.567302
Michel, J., Jordana, M.J., 1987. Nationwide Distribution of Ra-228, Ra-226, Rn-222, and U in Groundwater, in: Radon in Ground Water. CRC Press.
Moore, W.S., 1996. Large groundwater inputs to coastal waters revealed by 226 Ra enrichments. Nature 380, 612–614. https://doi.org/10.1038/380612a0
Nolan, J., Weber, K.A., 2015. Natural Uranium Contamination in Major U.S. Aquifers Linked to Nitrate. Environ. Sci. Technol. Lett. 2, 215–220. https://doi.org/10.1021/acs.estlett.5b00174
Oral, R., Pagano, G., Siciliano, A., Toscanesi, M., Gravina, M., Di Nunzio, A., Palumbo, A., Thomas, P.J., Tommasi, F., Burić, P., Lyons, D.M., Guida, M., Trifuoggi, M., 2019. Soil pollution and toxicity in an area affected by emissions from a bauxite processing plant and a power plant in Gardanne (southern France). Ecotoxicol. Environ. Saf. 170, 55–61. https://doi.org/10.1016/j.ecoenv.2018.11.122
Qian, Y., Jochens, A.E., Kennicutt II, M.C., Biggs, D.C., 2003. Spatial and temporal variability of phytoplankton biomass and community structure over the continental margin of the northeast Gulf of Mexico based on pigment analysis. Cont. Shelf Res. 23, 1–17. https://doi.org/10.1016/S0278-4343(02)00173-5
Qiu, Y.-W., Zhang, G., Liu, G.-Q., Guo, L.-L., Li, X.-D., Wai, O., 2009. Polycyclic aromatic hydrocarbons (PAHs) in the water column and sediment core of Deep Bay, South China. Estuar. Coast. Shelf Sci. 83, 60–66. https://doi.org/10.1016/j.ecss.2009.03.018
Reyna, N.E., Hardison, A., Liu, Z., 2017. Influence of major storm events on the quantity and composition of particulate organic matter and the phytoplankton community in a subtropical estuary, Texas. Front. Mar. Sci. 4, 43.
Santschi, P.H., Presley, B.J., Wade, T.L., Garcia-Romero, B., Baskaran, M., 2001. Historical contamination of PAHs, PCBs, DDTs, and heavy metals in Mississippi River Delta, Galveston Bay and Tampa Bay sediment cores. Mar. Environ. Res. 52, 51–79. https://doi.org/10.1016/S0141-1136(00)00260-9

Sun, M., Aller, R.C., Lee, C., 1991. Early diagenesis of chlorophyll-a in Long Island Sound sediments: A measure of carbon flux and particle reworking. J. Mar. Res. 49, 379–401. https://doi.org/10.1357/002224091784995927

Texas Commission on Environmental Quality, 2019. Preliminary Groundwater Assessment Report.

Wade, T.L., Soliman, Y., Sweet, S.T., Wolff, G.A., Presley, B.J., 2008. Trace elements and polycyclic aromatic hydrocarbons (PAHs) concentrations in deep Gulf of Mexico sediments. Deep Sea Res. Part II Top. Stud. Oceanogr., The Deep Gulf of Mexico Benthos Program 55, 2585–2593. https://doi.org/10.1016/j.dsr2.2008.07.006

Wang, Z., Liu, Z., Liu, M., Xu, K., Mayer, L.M., 2016. The impact of drying on structure of sedimentary organic matter in wetlands: Probing with native and amended polycyclic aromatic hydrocarbons. Sci. Total Environ. 568, 42–51. https://doi.org/10.1016/j.scitotenv.2016.05.184

Wang, Z., Liu, Z., Xu, K., Mayer, L.M., Zhang, Z., Kolker, A.S., Wu, W., 2014. Concentrations and sources of polycyclic aromatic hydrocarbons in surface coastal sediments of the northern Gulf of Mexico. Geochem. Trans. 15, 2. https://doi.org/10.1186/1467-4866-15-2

Wang, Z., Liu, Z., Yang, Y., Li, T., Liu, M., 2012. Distribution of PAHs in tissues of wetland plants and the surrounding sediments in the Chongming wetland, Shanghai, China. Chemosphere 89, 221–227. https://doi.org/10.1016/j.chemosphere.2012.04.019

Wilcke, W., 2007. Global patterns of polycyclic aromatic hydrocarbons (PAHs) in soil. Geoderma 141, 157–166. https://doi.org/10.1016/j.geoderma.2007.07.007

Xue, J., Lee, C., Wakeham, S.G., Armstrong, R.A., 2011. Using principal components analysis (PCA) with cluster analysis to study the organic geochemistry of sinking particles in the ocean. Org. Geochem. 42, 356–367. https://doi.org/10.1016/j.orggeochem.2011.01.012

Yang, Z., Feng, J., Niu, J., Shen, Z., 2008. Release of polycyclic aromatic hydrocarbons from Yangtze River sediment cores during periods of simulated resuspension. Environ. Pollut. 155, 366–374. https://doi.org/10.1016/j.envpol.2007.11.007

Yunker, M.B., Macdonald, R.W., Veltkamp, D.J., Cretney, W.J., 1995. Terrestrial and marine biomarkers in a seasonally ice-covered Arctic estuary — integration of multivariate and biomarker approaches. Mar. Chem. 49, 1–50. https://doi.org/10.1016/0304-4203(94)00057-K

Yunker, M.B., Macdonald, R.W., Vingarzan, R., Mitchell, R.H., Goyette, D., Sylvestre, S., 2002. PAHs in the Fraser River basin: a critical appraisal of PAH ratios as indicators of PAH source and composition. Org. Geochem. 33, 489–515. https://doi.org/10.1016/S0146-6380(02)00002-5

Zhao, N., Tan, Y., Zhang, X., Zhen, Z., Song, Q., Ju, F., Ling, H., 2023. Molecular Insights on the Adsorption of Polycyclic Aromatic Hydrocarbons on Soil Clay Minerals. Environ. Eng. Sci. 40, 105–113. https://doi.org/10.1089/ees.2022.0190

Zhu, L., Shi, W., Zhou, J., Yu, J., Kong, L., Qin, B., 2021. Strong turbulence accelerates sediment nitrification-denitrification for nitrogen loss in shallow lakes. Sci. Total Environ. 761, 143210. https://doi.org/10.1016/j.scitotenv.2020.143210

Figures

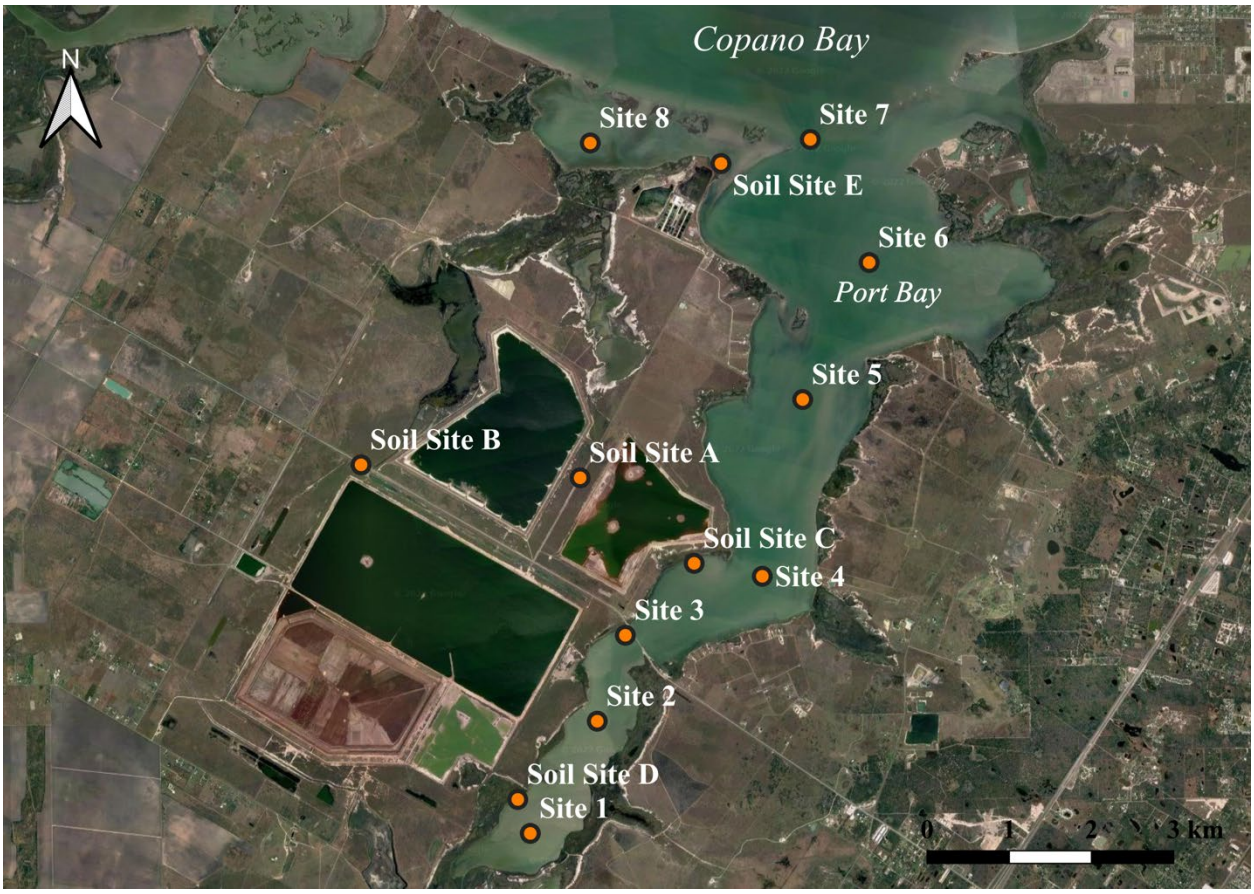

Figure 1. Sampling sites in Port Bay. Soil sites A to E are for soil and groundwater samples, while sites 1 to 8 are for surface water and surface sediment samples in the bay. In addition, Oyster samples are also collected at sites 3, 4, 7, and 8.

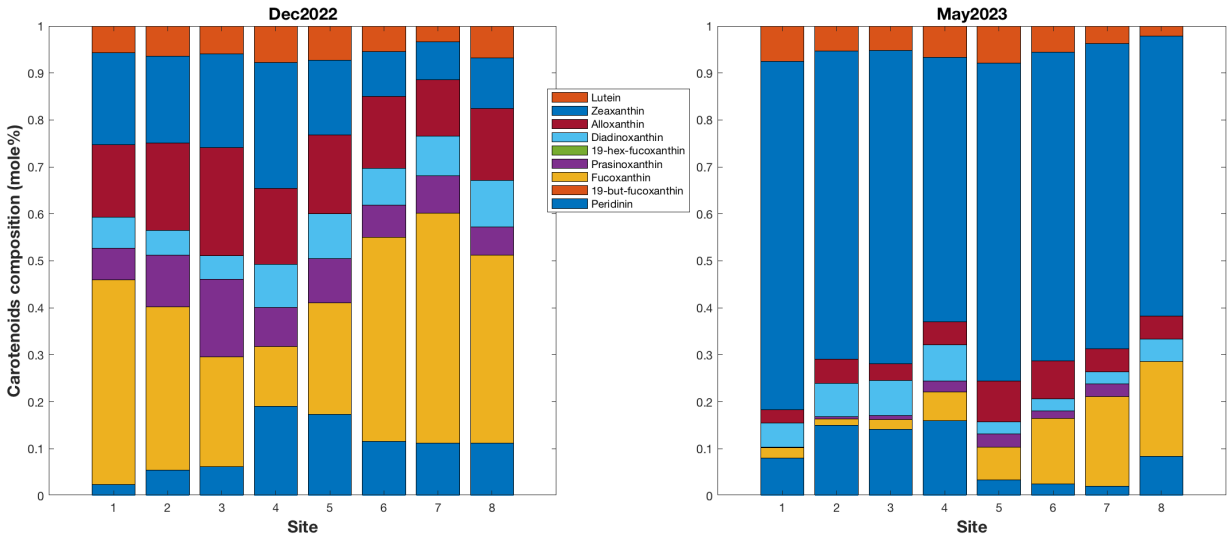

Figure 2. The carotenoids pigment composition at different sites in different sampling times.

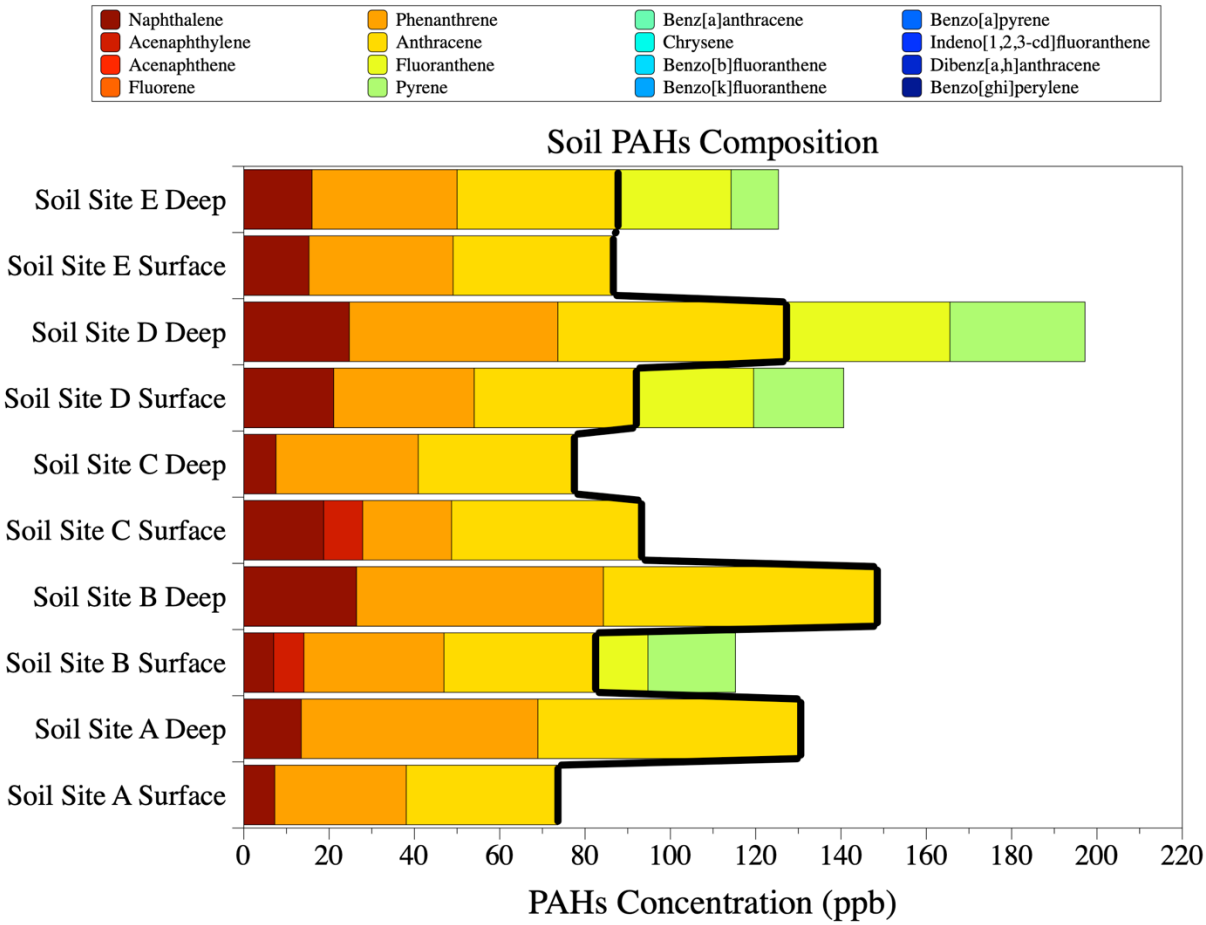

Figure 3. PAH concentration and composition from the 5 terrestrial sites near the tailings ponds. PAHs to the left of the black line are low molecular weight ones, while those to the right of the black line are high molecular weight ones.

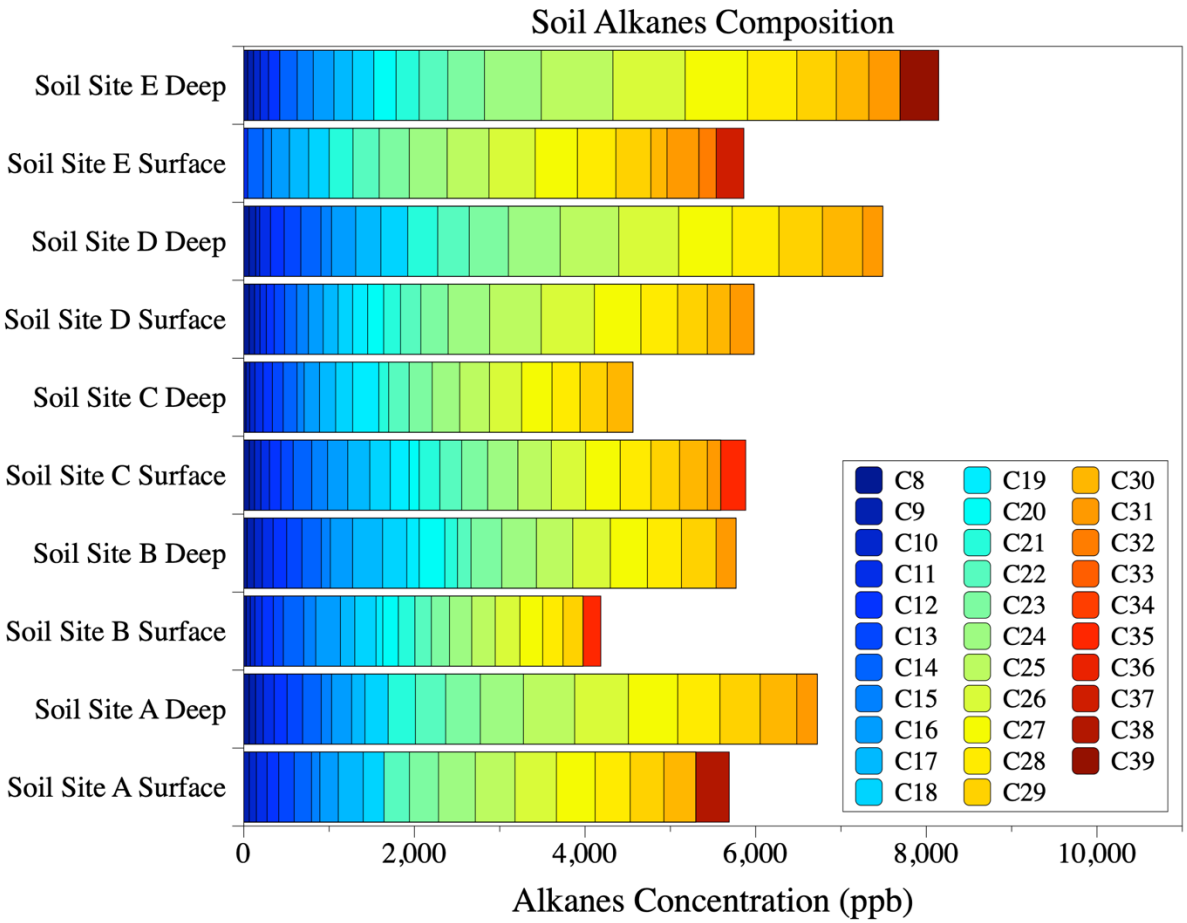

Figure 4. n-Alkanes concentration and composition of samples from the 5 terrestrial sites near the tailings ponds.

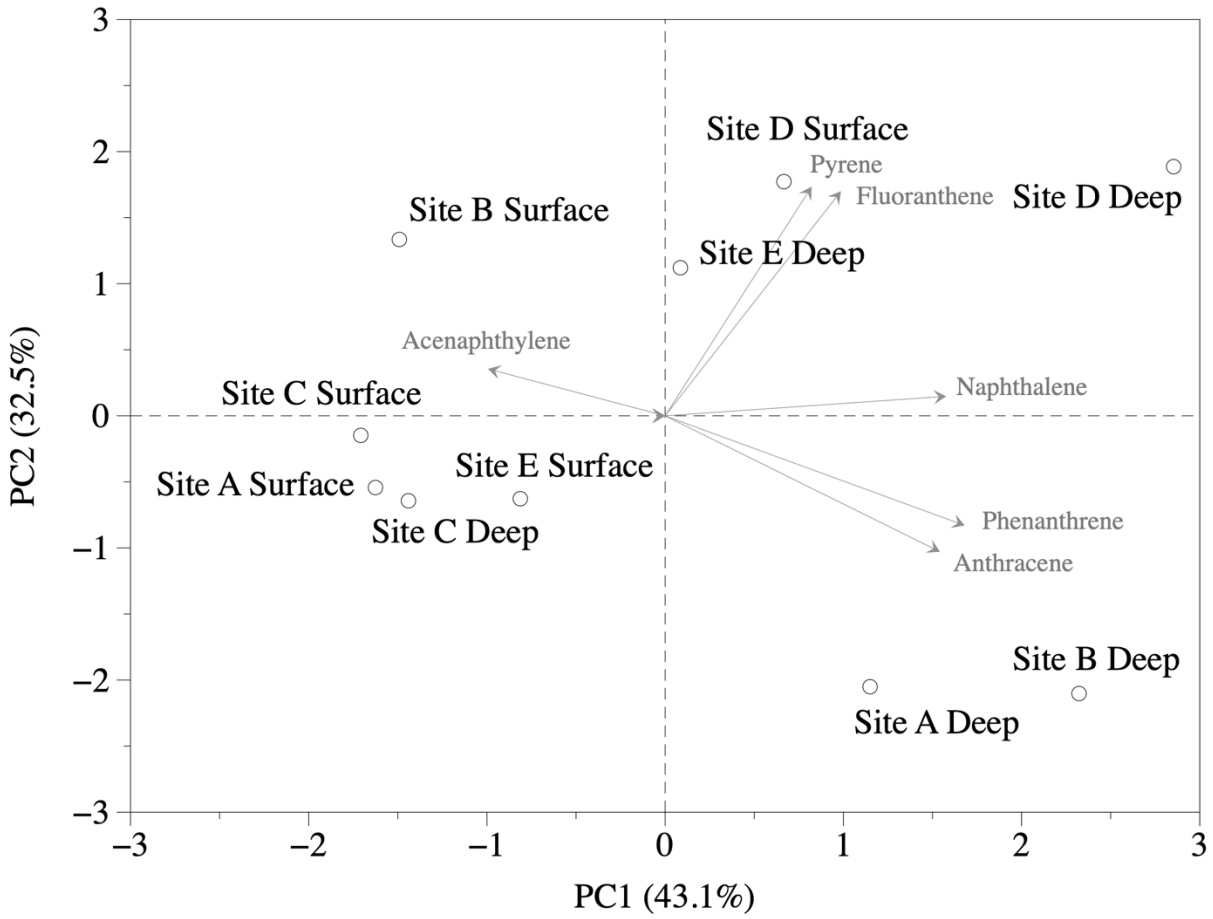

Figure 5. Principal component analysis (PCA) based on the composition of PAHs, with PC 1 explaining 43.1% of the variance, and PC2 32.5% of the rest.

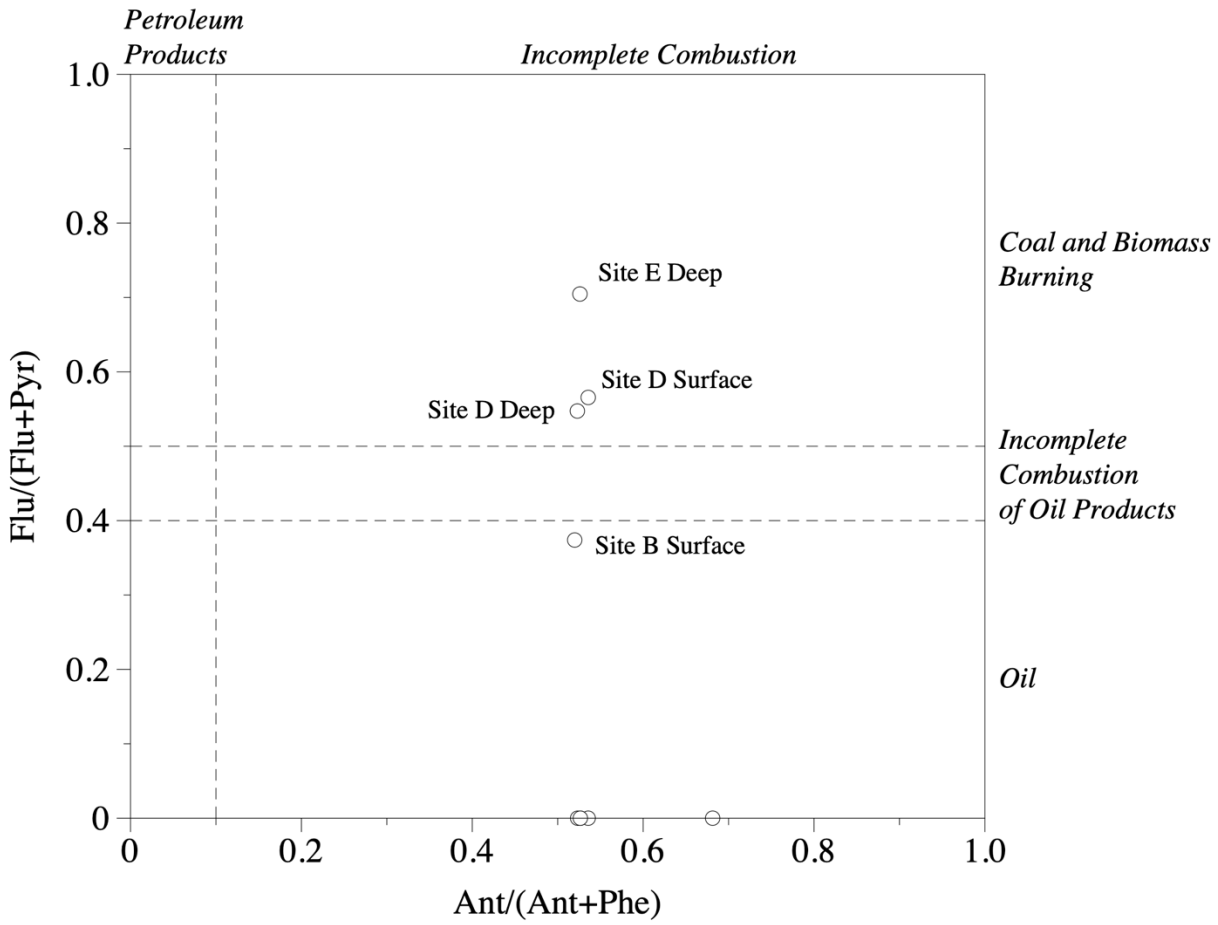

Figure 6. Diagnostics for distinguishing possible sources of PAHs from soil sites.

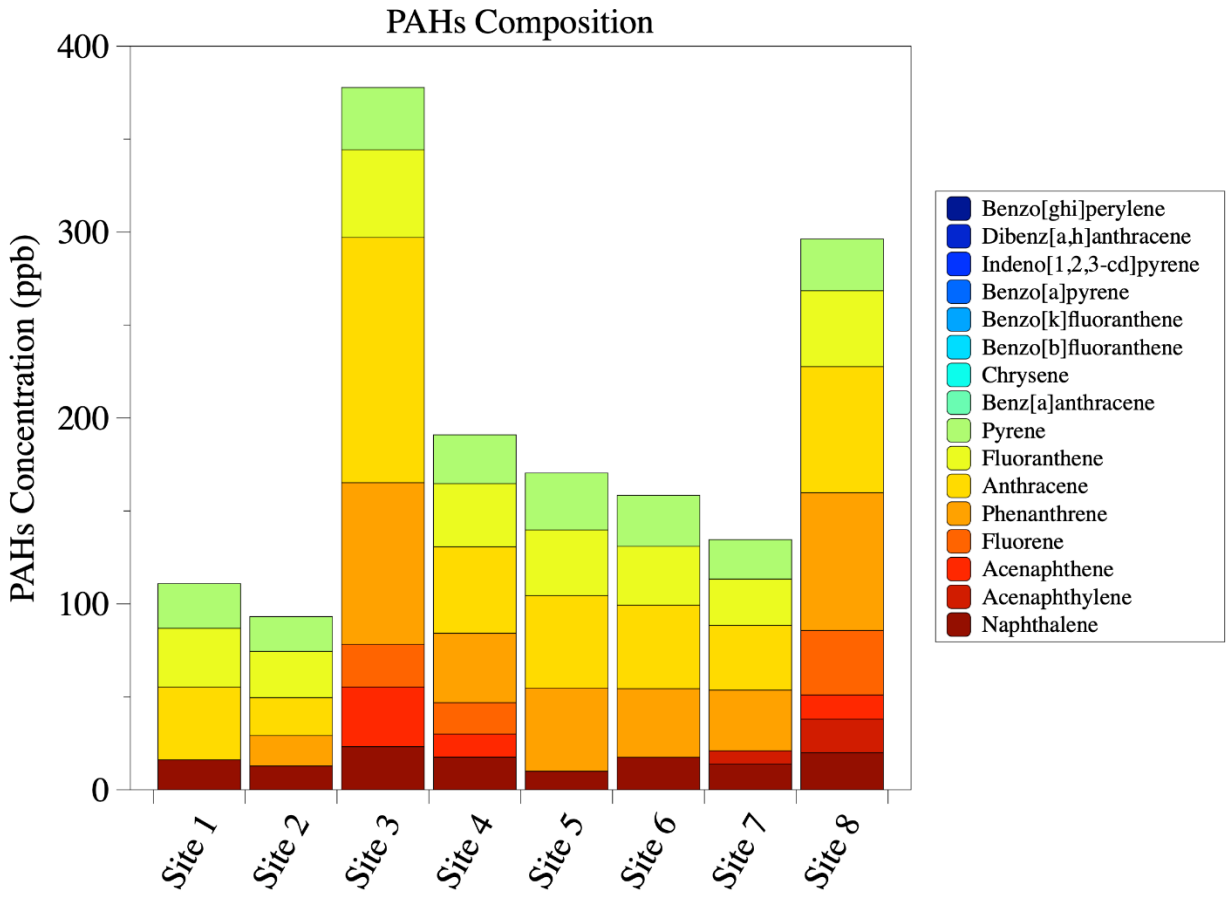

Figure 7. PAHs concentration and composition from the bay surface sediment (5 cm) of 8 sites in Port Bay (Dec-2022).

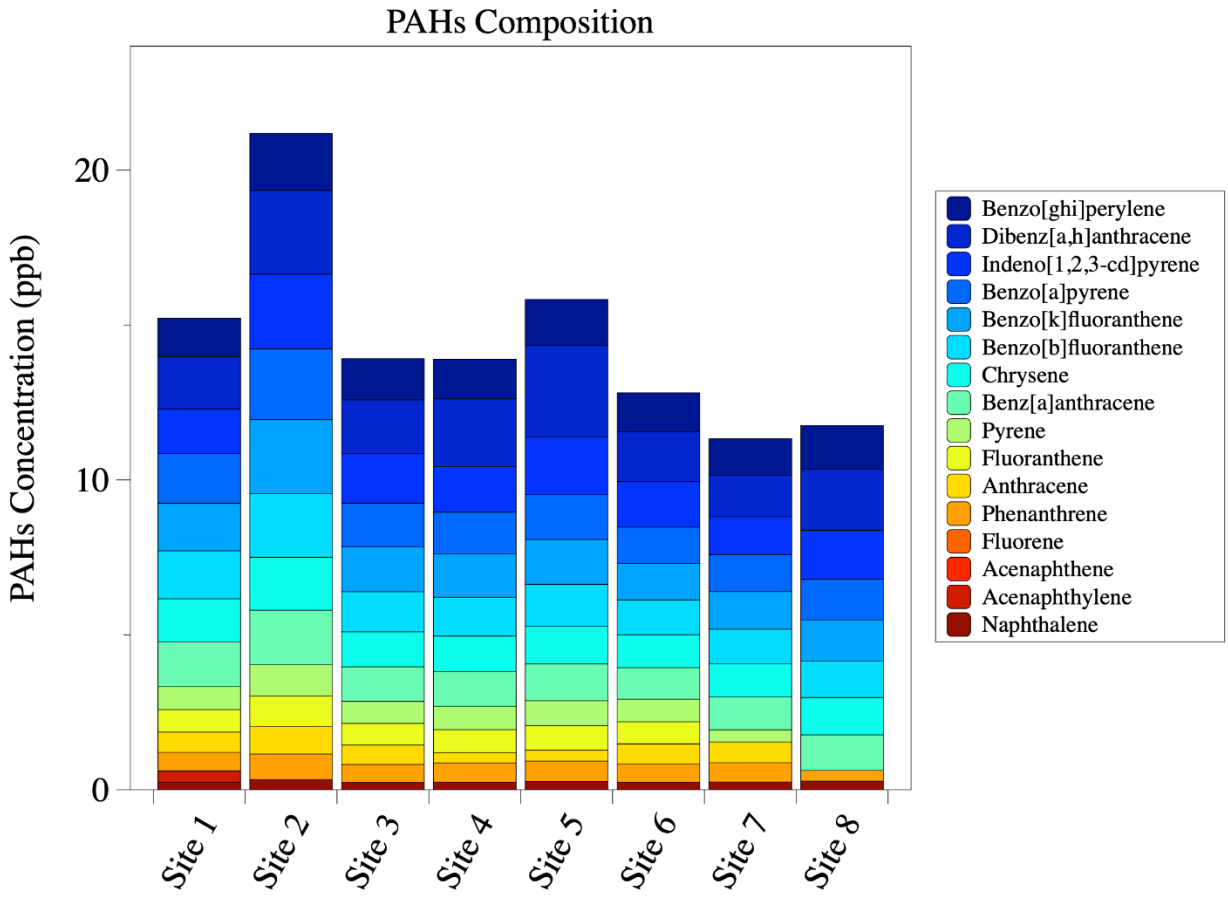

Figure 8. PAHs concentration and composition from surface water at 8 sites in Port Bay (Dec-2022).

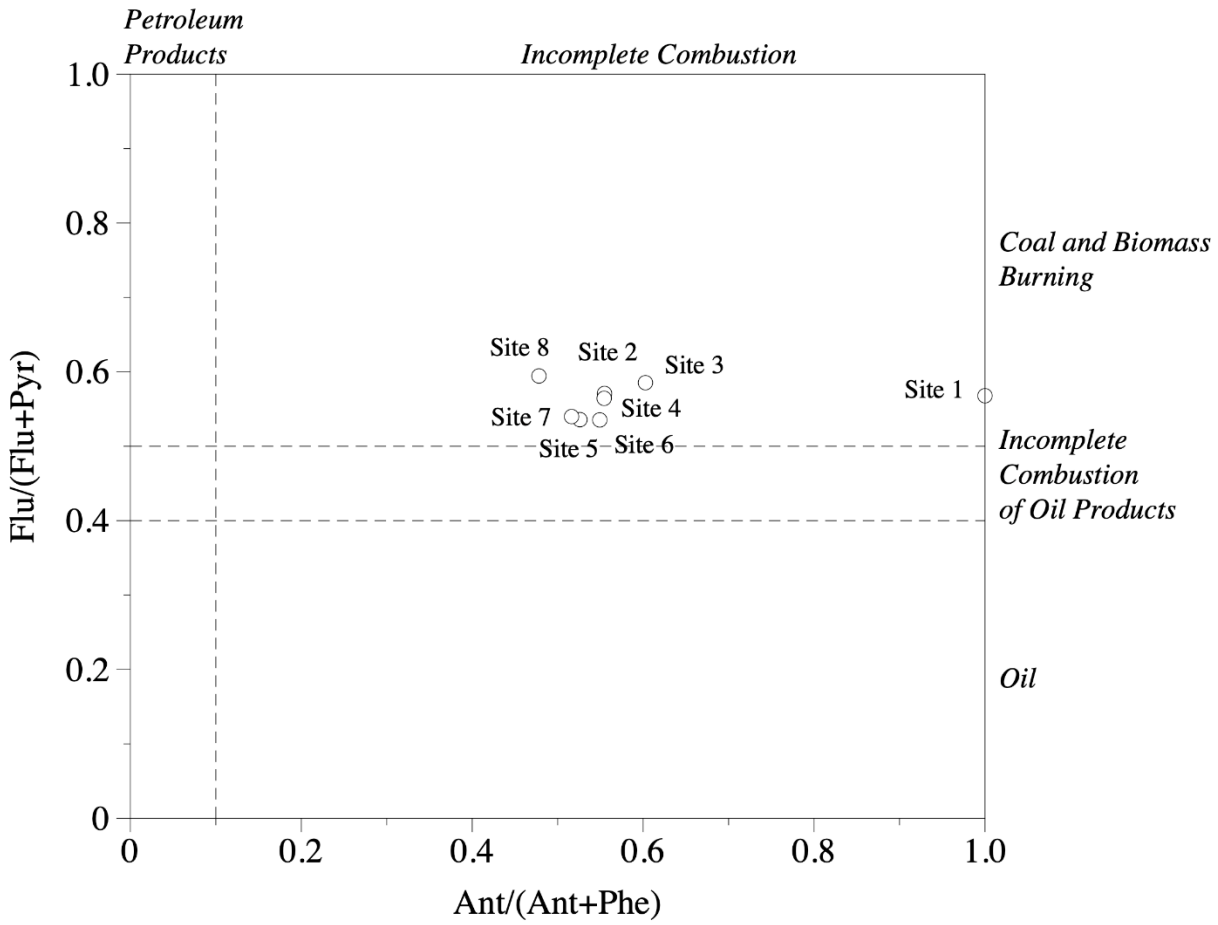

Figure 9. Diagnostics for distinguishing possible sources of PAHs from bay surface sediments.

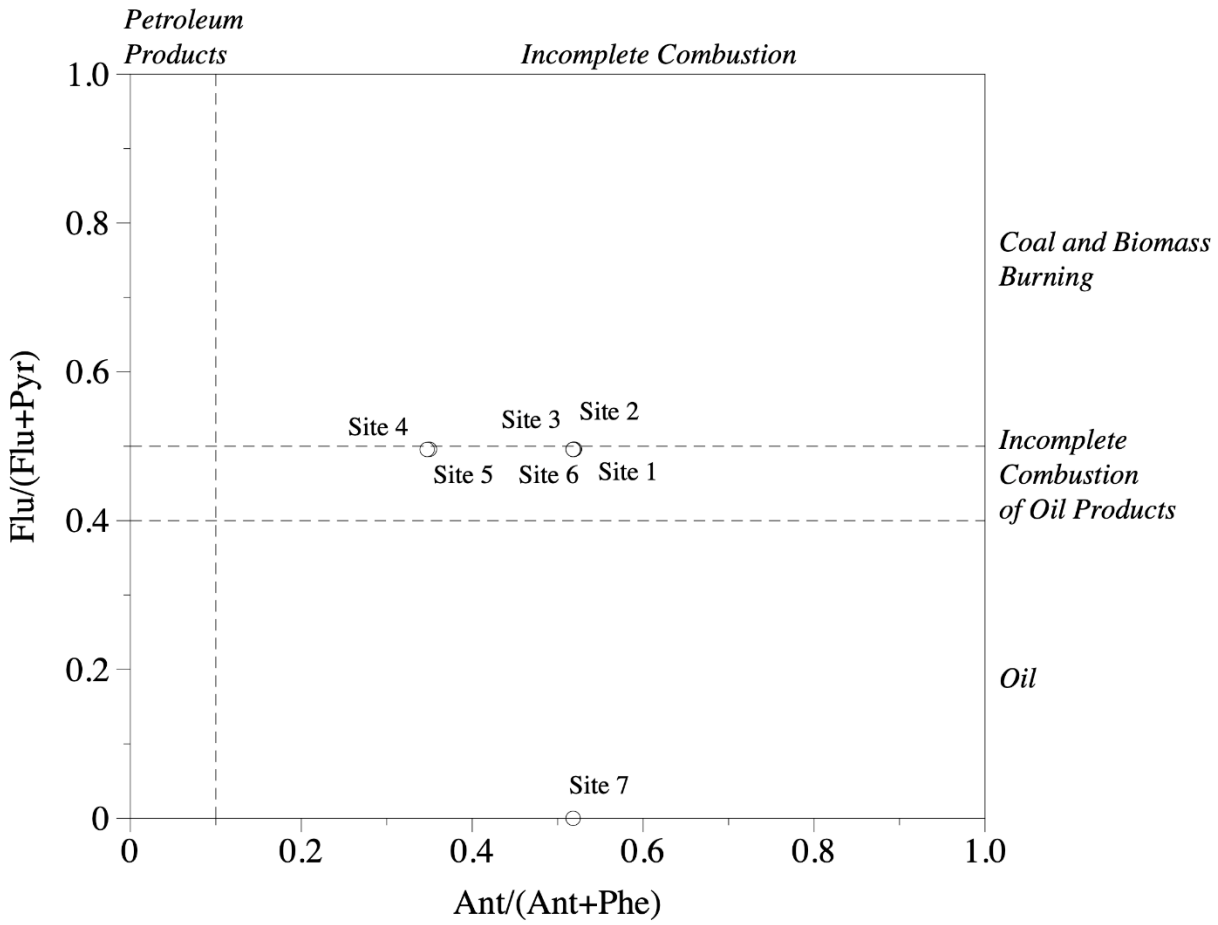

Figure 10. Diagnostics for distinguishing possible sources of PAHs from Port Bay surface waters.

Tables

Table 1. Concentrations of Hg in oyster tissue

Samples	[tHg] Whole Oyster (mg/kg) WW	Site Average (mg/kg) WW	E.U. EQS Biota	HQ Max	HQ Average
Site 3 A	0.019	0.02	0.02	1.05	0.98
Site 3 B	0.019				
Site 3 C	0.021				
Site 4 A	0.012	0.01	0.02	0.70	0.63
Site 4 B	0.012				
Site 4 C	0.014				
Site 7 A	0.007	0.01	0.02	0.42	0.38
Site 7 B	0.008				
Site 7 C	0.007				
Site 8 A	0.011	0.01	0.02	0.60	0.57
Site 8 B	0.011				
Site 8 C	0.012				

Table 2. Mercury (Hg), Arsenic (As) and Chromium (Cr) concentrations in Port Bay surface waters. Error bars represent the standard deviation of duplicate samples.

Sample	Hg (mg/L)	As (mg/L)	Cr (mg/L)
Site 3	N.D.	0.008 ± 0.004	N.D.
Site 4	N.D.	N.D.	N.D.
Site 5	N.D.	N.D.	N.D.
Site 6	N.D.	N.D.	N.D.
Site 7	N.D.	N.D.	N.D.
Site 8	N.D.	N.D.	N.D.

N.D.: not detected. The method detection limit is 0.0001 mg/L for Hg, 0.004 mg/L for As and 0.0007 mg/L for Cr.

Table 3. Nutrient concentrations in Port Bay surface waters. Error bars represent the standard deviation of duplicate samples.

Sites	12-2022			05-2023			11-2023		
	NH_4^+ (ppb)	PO_4^{3-} (ppb)	NO_x (ppb)	NH_4^+ (ppb)	PO_4^{3-} (ppb)	NO_x (ppb)	NH_4^+ (ppb)	PO_4^{3-} (ppb)	NO_x (ppb)
Site 1	3.78 ± 0.26	22.26 ± 0.69	N.D.	3.90 ± 1.15	102.85 ± 1.85	25.23 ± 1.55	-	-	-
Site 2	23.48 ± 0.51	36.4 ± 1.68	N.D.	3.77 ± 1.40	73.00 ± 0.86	21.66 ± 4.55	-	-	-
Site 3	38.03 ± 0.29	46.98 ± 1.15	N.D.	3.13 ± 0.48	62.36 ± 1.02	28.13 ± 3.78	12.84 ± 0.03	139.65 ± 1.65	0.16 ± 0.00
Site 4	33.02 ± 0.04	67.55 ± 3.40	N.D.	1.25 ± 0.42	N.D.	43.28 ± 12.27	8.85 ± 0.60	N.D.	N.D.
Site 5	28.9 ± 0.11	65.8 ± 2.52	N.D.	1.36 ± 0.39	N.D.	40.29 ± 3.00	7.59 ± 0.96	N.D.	N.D.
Site 6	11.21 ± 0.25	66.34 ± 5.07	N.D.	8.64 ± 0.17	N.D.	42.12 ± 5.13	7.76 ± 0.10	0.55 ± 0.55	N.D.
Site 7	8.69 ± 0.17	78.27 ± 1.06	N.D.	7.82 ± 0.37	0.87 ± 1.39	35.09 ± 9.18	7.46 ± 0.06	0.18 ± 0.18	N.D.
Site 8	35.13 ± 0.38	82.6 ± 6.61	N.D.	10.42 ± 0.18	N.D.	38 ± 5.17	6.66 ± 0.39	30.17 ± 0.41	N.D.

N.D.: not detected.

-: no sample collected.

Table 4. Total suspended solids (mg/L) in Port Bay surface waters in November 2023. Error bars represent the standard deviation of duplicate samples.

Sites	Total suspended solids (TSS; mg/L)
Site 3	63.1 ± 0.8
Site 4	87.5 ± 1.4
Site 5	99.7 ± 2.0
Site 6	104.4 ± 2.0
Site 7	104.1 ± 5.0
Site 8	84.7 ± 4.6

Table 5. The individual pigment concentrations (ng/L) in the Port Bay surface water collected in different sampling sites and dates. Error bars represent the standard deviation of duplicate samples.

Pigments	**Site 1**	**Site 2**	**Site 3**	**Site 4**	**Site 5**	**Site 6**	**Site 7**	**Site 8**
Sampling date	12-2022	12-2022	12-2022	12-2022	12-2022	12-2022	12-2022	12-2022
Chlorophyll c2	44±12	32±3	25±6	20±8	15±2	36±13	24±2	23±12
Pheophorbide a	334±106	100±57	82±72	34±17	42±0	108±7	37±9	120±2
Chlolophyll b	861±85	781±122	662±138	312±80	330±27	500±40	347±42	392±71
Divinyl Chlorophyll a	14±4	14±3	12±4	5±2	5±3	10±6	6±1	3±0
Chlorophyll a	6674±268	4526±700	3220±903	1709±432	1711±195	3333±364	1985±329	2630±407
Pheophytin	329±20	244±74	202±51	78±32	70±16	134±28	69±35	135±19
Peridinin	54±77	90±17	67±32	90±22	77±9	114±10	68±2	87±1
19-but-fucoxanthin	0	0	0	0	0	0	0	0
Fucoxanthin	1009±8	602±121	265±85	63±27	111±33	446±105	312±66	324±41
Prasinoxanthin	141±16	174±32	172±28	38±9	40±5	64±15	46±7	44±2
19-hex-fucoxanthin	0	0	0	0	0	0	0	0
Diadinoxanthin	136±1	82±15	50±4	40±12	40±5	71±7	48±10	71±4
Alloxanthin	305±22	275±42	223±78	68±14	67±3	135±13	66±13	106±4
Zeaxanthin	393±26	276±51	195±44	115±28	65±6	85±2	44±9	75±8
Lutein	113±29	97±15	58±3	33±9	29±3	48±1	18±5	48±5

Continued

Pigments	**Site 1**	**Site 2**	**Site 3**	**Site 4**	**Site 5**	**Site 6**	**Site 7**	**Site 8**
Sampling date	05-2023	05-2023	05-2023	05-2023	05-2023	05-2023	05-2023	06-2023
Chlorophyll c2	33±31	81±2	56±15	60±5	21±4	17±5	13±2	44±4
Pheophorbide a	88±9	107±21	85±42	29±7	33±2	20±4	29±3	62±8
Chlolophyll b	580±276	485±42	364±10	420±11	347±18	271±2	197±16	284±15
Divinyl Chlorophyll a	14±4	19±7	13±5	8±2	7±1	6±2	5±0	8±1
Chlorophyll a	6406±1788	7762±521	5961±310	3694±315	2437±123	1862±31	1549±133	3759±153
Pheophytin	357±72	380±24	327±18	119±9	101±16	63±11	93±10	174±2
Peridinin	274±281	585±220	432±6	270±94	46±16	24±5	18±2	154±39
19-but-fucoxanthin	0	0	0	0	0	0	0	0
Fucoxanthin	76±34	58±28	68±4	110±26	98±27	137±59	179±13	388±46
Prasinoxanthin	5±7	19±1	26±9	37±4	36±13	15±4	23±3	0
19-hex-fucoxanthin	0	0	0	0	0	0	0	0
Diadinoxanthin	162±126	254±20	209±16	121±9	32±2	22±4	21±6	81±13
Alloxanthin	83±27	180±18	99±8	73±3	106±13	68±11	40±6	82±8
Zeaxanthin	2267±159	2312±132	1839±96	860±50	827±20	556±44	527±67	987±3
Lutein	229±40	186±4	143±2	102±5	96±9	47±6	30±5	36±1

Table 6. Concentration of PAHs at the 5 terrestrial sites. Unit: ppb or ng/g dried weight sediment. Surface refers to the depth of 0.05m, while deep refers to ~1 m. Error bars represent the standard deviation of duplicate samples.

PAHs (ppb)	Site A Surface	Site A Deep	Site B Surface	Site B Deep	Site C Surface	Site C Deep	Site D Surface	Site D Deep	Site E Surface	Site E Deep
Naphthalene	7.3 ± 10.3	13.5 ± 19.0	7.0 ± 9.9	26.4 ± 0.8	18.7 ± 0.2	7.6 ± 10.7	21.1 ± 0.6	24.7 ± 0.1	15.3 ± 0.2	16.0 ± 0.0
Acenaphthylene	0 ± 0	0 ± 0	7.1 ± 10.1	0 ± 0	9.1 ± 12.9	0 ± 0	0 ± 0	0 ± 0	0 ± 0	0 ± 0
Acenaphthene	0 ± 0	0 ± 0	0 ± 0	0 ± 0	0 ± 0	0 ± 0	0 ± 0	0 ± 0	0 ± 0	0 ± 0
Fluorene	0 ± 0	0 ± 0	0 ± 0	0 ± 0	0 ± 0	0 ± 0	0 ± 0	0 ± 0	0 ± 0	0 ± 0
Phenanthrene	30.8 ± 0.9	55.5 ± 4.3	32.8 ± 0.3	57.9 ± 2.8	20.8 ± 29.5	33.3 ± 0.1	32.9 ± 1.1	48.9 ± 0.3	33.8 ± 0.9	34 ± 0.8
Anthracene	35.6 ± 0.3	61.6 ± 3.7	35.6 ± 0.2	64.2 ± 3.1	44.5 ± 0.1	36.6 ± 0.1	38.0 ± 2.2	53.6 ± 1.6	37.6 ± 1.1	37.7 ± 0.8
Fluoranthene	0 ± 0	0 ± 0	12.3 ± 17.3	0 ± 0	0 ± 0	0 ± 0	27.5 ± 1.0	38.3 ± 1.1	0 ± 0	26.5 ± 1.0
Pyrene	0 ± 0	0 ± 0	20.5 ± 0.2	0 ± 0	0 ± 0	0 ± 0	21.1 ± 0.6	31.7 ± 0.0	0 ± 0	11.1 ± 15.7
Benz[a]anthracene	0 ± 0	0 ± 0	0 ± 0	0 ± 0	0 ± 0	0 ± 0	0 ± 0	0 ± 0	0 ± 0	0 ± 0
Chrysene	0 ± 0	0 ± 0	0 ± 0	0 ± 0	0 ± 0	0 ± 0	0 ± 0	0 ± 0	0 ± 0	0 ± 0
Benzo[b]fluoranthene	0 ± 0	0 ± 0	0 ± 0	0 ± 0	0 ± 0	0 ± 0	0 ± 0	0 ± 0	0 ± 0	0 ± 0
Benzo[k]fluoranthene	0 ± 0	0 ± 0	0 ± 0	0 ± 0	0 ± 0	0 ± 0	0 ± 0	0 ± 0	0 ± 0	0 ± 0
Benzo[a]pyrene	0 ± 0	0 ± 0	0 ± 0	0 ± 0	0 ± 0	0 ± 0	0 ± 0	0 ± 0	0 ± 0	0 ± 0
Indeno[1,2,3-cd]pyrene	0 ± 0	0 ± 0	0 ± 0	0 ± 0	0 ± 0	0 ± 0	0 ± 0	0 ± 0	0 ± 0	0 ± 0
Dibenz[a,h]anthracene	0 ± 0	0 ± 0	0 ± 0	0 ± 0	0 ± 0	0 ± 0	0 ± 0	0 ± 0	0 ± 0	0 ± 0
Benzo[ghi]perylene	0 ± 0	0 ± 0	0 ± 0	0 ± 0	0 ± 0	0 ± 0	0 ± 0	0 ± 0	0 ± 0	0 ± 0

Table 7. Concentration of *n*-Alkanes at the 5 terrestrial sites. Unit: ppb or ng/g dried weight sediment. Surface refers to the depth of 0.05m, while deep refers to ~1m. Error bars represent the standard deviation of duplicate samples.

n-Alkanes (ppb)	Site A Surface	Site A Deep	Site B Surface	Site B Deep	Site C Surface	Site C Deep	Site D Surface	Site D Deep	Site E Surface	Site E Deep
C8	0 ± 0	63.6 ± 4.7	27.8 ± 39.3	37.8 ± 53.4	65.3 ± 5.5	25 ± 0.6	64.3 ± 2.3	63.1 ± 5.6	0 ± 0	45.5 ± 2.6
C9	64.0 ± 4.1	74.8 ± 3.4	48.7 ± 4.0	83.9 ± 2.7	60.9 ± 9.5	44.6 ± 0.0	62.1 ± 1.4	76.7 ± 9.9	0 ± 0	68.8 ± 2.7
C10	83.3 ± 1.8	89.3 ± 2.7	53.0 ± 1.3	94.8 ± 7.8	73.9 ± 4.1	60.2 ± 2.5	63.2 ± 3.7	46.0 ± 65.1	0 ± 0	77 ± 0.6
C11	125.4 ± 4.8	127.8 ± 32.9	84.2 ± 4.1	126.7 ± 3.1	100.3 ± 3.4	95.7 ± 5.6	73.8 ± 5.7	127.5 ± 9.1	46.1 ± 65.2	98.1 ± 6.8
C12	137.1 ± 0.8	151.5 ± 15.3	132.1 ± 0.5	158.8 ± 3.4	133.4 ± 3.7	108.8 ± 1.9	92.8 ± 2.6	160.2 ± 7.9	0 ± 0	131.9 ± 8.9
C13	180.4 ± 1.8	182.1 ± 27.8	117.6 ± 3.9	179.7 ± 6.5	144.5 ± 11.1	127.0 ± 0.5	122.3 ± 1.5	194.3 ± 13.0	0 ± 0	0 ± 0
C14	203.8 ± 5.1	218.3 ± 17.3	238.9 ± 0.7	226.3 ± 10.8	218.5 ± 7.4	162.7 ± 5.2	141.0 ± 9.2	236.2 ± 4.6	180.9 ± 5.4	204.8 ± 8.0
C15	97.4 ± 137.8	122.1 ± 172.6	141.1 ± 6.5	106.8 ± 151.0	184.7 ± 11.1	83.1 ± 117.5	137.3 ± 5.5	124.6 ± 176.2	97.6 ± 138.1	187.7 ± 9.3
C16	216.4 ± 2.9	234.7 ± 24	289.2 ± 14.0	260.3 ± 10.1	236.7 ± 3.6	180.6 ± 0.6	173.3 ± 0.8	282.3 ± 11.6	210.1 ± 5.6	242.7 ± 2.8
C17	291.6 ± 101.5	155.7 ± 220.2	167.8 ± 0.4	351.3 ± 152.4	258.5 ± 11.8	188.7 ± 3.4	175.6 ± 0.7	295.7 ± 6.0	225.2 ± 7.7	217.5 ± 10.1
C18	244.1 ± 0.5	271.7 ± 26.1	249.6 ± 5.5	284.3 ± 20.0	239.6 ± 17.4	199.5 ± 0.5	170.3 ± 16.3	314.7 ± 3.6	240.2 ± 5.0	250 ± 6.1
C19	0 ± 0	0 ± 0	78.8 ± 111.4	144.8 ± 204.8	221 ± 8.5	307.1 ± 0.8	175.8 ± 3.1	0 ± 0	0 ± 0	0 ± 0
C20	0 ± 0	0 ± 0	182.7 ± 7.3	300.5 ± 15.6	118.3 ± 167.3	0 ± 0	187.6 ± 12.2	0 ± 0	0 ± 0	260.7 ± 1.1
C21	0 ± 0	319.6 ± 31.8	194.4 ± 0.7	148.3 ± 209.7	242.2 ± 8.9	114.7 ± 162.2	198.0 ± 9.0	351.3 ± 9.1	279.5 ± 21.9	270.5 ± 0.7
C22	297.4 ± 0.8	354.6 ± 38.3	192.4 ± 7.2	158.9 ± 224.7	256.0 ± 13.4	239.6 ± 5.2	237.6 ± 17.9	369.9 ± 6.2	307.0 ± 18.3	335.9 ± 13.7
C23	341.4 ± 7.4	406.2 ± 42.3	213.1 ± 5.7	360.1 ± 23.9	304.4 ± 16.5	270.4 ± 1.9	320.2 ± 18.6	459.1 ± 9.8	352.3 ± 13.7	429.5 ± 33.0
C24	431.4 ± 26.2	505.7 ± 45.5	260.2 ± 14	406.6 ± 41.2	354.5 ± 14.8	322.6 ± 12.4	486.7 ± 10.6	606.3 ± 16.3	444.6 ± 15.5	665.3 ± 31.8
C25	464.9 ± 35.5	600.0 ± 51.2	276.1 ± 15.9	426.1 ± 19.4	392.3 ± 31.7	349.6 ± 18.1	603.6 ± 10.2	687.0 ± 12.1	490.2 ± 4.7	840.4 ± 46.0
C26	485.6 ± 35.6	630.3 ± 51.4	288.5 ± 13.5	440.2 ± 23.1	401.9 ± 24.2	376.7 ± 7.4	623.2 ± 36.3	702.3 ± 67.5	541.4 ± 52.3	846.7 ± 24.9
C27	453.6 ± 23.3	578.1 ± 19.8	267.4 ± 13.5	433.8 ± 27.5	404.3 ± 20.9	356.0 ± 19.2	545.9 ± 22.3	626.5 ± 75.2	495.2 ± 0.3	730.8 ± 63.4
C28	410.9 ± 11.2	495 ± 29.2	238.1 ± 2.6	399.8 ± 7.1	360.7 ± 9.4	328.3 ± 8.3	430.2 ± 9.8	548 ± 6.9	450.6 ± 17	578.4 ± 20.1
C29	395.0 ± 10.9	471.1 ± 54.9	235.6 ± 10	406.4 ± 21.9	335.4 ± 44.1	318 ± 12.9	348.5 ± 9.8	510.5 ± 42.9	410.1 ± 34.1	462.7 ± 7.9
C30	374.9 ± 2.7	429.4 ± 36.6	0 ± 0	0 ± 0	326 ± 30.3	303.2 ± 8.6	266.9 ± 31.8	471.2 ± 9.3	189.1 ± 267.4	380.9 ± 20.0
C31	0 ± 0	240.6 ± 340.3	0 ± 0	234.3 ± 331.3	157.6 ± 222.9	0 ± 0	281.1 ± 1.8	236.2 ± 334.0	374.6 ± 5.2	365.9 ± 5.1
C32	0 ± 0	0 ± 0	0 ± 0	0 ± 0	0 ± 0	0 ± 0	0 ± 0	0 ± 0	201.9 ± 285.6	0 ± 0
C33	0 ± 0	0 ± 0	0 ± 0	0 ± 0	0 ± 0	0 ± 0	0 ± 0	0 ± 0	0 ± 0	0 ± 0
C34	0 ± 0	0 ± 0	0 ± 0	0 ± 0	0 ± 0	0 ± 0	0 ± 0	0 ± 0	0 ± 0	0 ± 0

Continued

n-Alkanes (ppb)	Site A Surface	Site A Deep	Site B Surface	Site B Deep	Site C Surface	Site C Deep	Site D Surface	Site D Deep	Site E Surface	Site E Deep
C35	0 ± 0	0 ± 0	207.8 ± 293.8	0 ± 0	292.2 ± 413.3	0 ± 0	0 ± 0	0 ± 0	0 ± 0	0 ± 0
C36	0 ± 0	0 ± 0	0 ± 0	0 ± 0	0 ± 0	0 ± 0	0 ± 0	0 ± 0	0 ± 0	0 ± 0
C37	0 ± 0	0 ± 0	0 ± 0	0 ± 0	0 ± 0	0 ± 0	0 ± 0	0 ± 0	324.6 ± 459.0	0 ± 0
C38	390.8 ± 552.7	0 ± 0	0 ± 0	0 ± 0	0 ± 0	0 ± 0	0 ± 0	0 ± 0	0 ± 0	0 ± 0
C39	0 ± 0	0 ± 0	0 ± 0	0 ± 0	0 ± 0	0 ± 0	0 ± 0	0 ± 0	0 ± 0	453.3 ± 641.1

Table 8. Concentration of PAHs in surface sediments at 8 bay sites (December 2022). Unit: ppb or ng/g dried weight sediment. Error bars represent the standard deviation of duplicate samples.

PAHs (ppb)	Site 1	Site 2	Site 3	Site 4	Site 5	Site 6	Site 7	Site 8
Naphthalene	16.1 ± 0.9	12.8 ± 0.0	23.2 ± 0.9	17.6 ± 0.4	10.0 ± 10.0	17.5 ± 0.1	13.9 ± 0.1	19.9 ± 3.6
Acenaphthylene	0.0 ± 0.0	0.0 ± 0.0	0.0 ± 0.0	0.0 ± 0.0	0.0 ± 0.0	0.0 ± 0.0	7.1 ± 7.1	18.1 ± 0.0
Acenaphthene	0.0 ± 0.0	0.0 ± 0.0	32.1 ± 2.2	12.4 ± 12.4	0.0 ± 0.0	0.0 ± 0.0	0.0 ± 0.0	13.0 ± 13.0
Fluorene	0.0 ± 0.0	0.0 ± 0.0	22.9 ± 22.9	16.9 ± 16.9	0.0 ± 0.0	0.0 ± 0.0	0.0 ± 0.0	34.7 ± 1.3
Phenanthrene	1.2 ± 0.1	1.5 ± 0.0	1.0 ± 0.1	1.1 ± 0.0	0.9 ± 0.0	1.0 ± 0.0	1.3 ± 0.0	1.2 ± 0.0
Anthracene	0.0 ± 0.0	16.4 ± 16.4	87.0 ± 4.2	37.3 ± 0.3	44.8 ± 0.3	36.9 ± 0.4	32.6 ± 0.4	74.1 ± 1.1
Fluoranthene	39.1 ± 2.0	20.4 ± 20.4	131.9 ± 4.7	46.5 ± 0.4	49.7 ± 0.1	44.9 ± 0.8	34.8 ± 0.3	67.9 ± 1.9
Pyrene	31.6 ± 0.4	24.9 ± 0.4	47.2 ± 1.8	34.0 ± 0.6	35.3 ± 0.3	31.6 ± 1.9	24.9 ± 0.2	40.8 ± 0.2
Benz[a]anthracene	24.1 ± 0.6	18.7 ± 0.4	33.4 ± 1.5	26.3 ± 1.2	30.6 ± 1.1	27.5 ± 0.0	21.2 ± 0.0	27.9 ± 0.1
Chrysene	0.0 ± 0.0	0.0 ± 0.0	0.0 ± 0.0	0.0 ± 0.0	0.0 ± 0.0	0.0 ± 0.0	0.0 ± 0.0	0.0 ± 0.0
Benzo[b]fluoranthene	0.0 ± 0.0	0.0 ± 0.0	0.0 ± 0.0	0.0 ± 0.0	0.0 ± 0.0	0.0 ± 0.0	0.0 ± 0.0	0.0 ± 0.0
Benzo[k]fluoranthene	0.0 ± 0.0	0.0 ± 0.0	0.0 ± 0.0	0.0 ± 0.0	0.0 ± 0.0	0.0 ± 0.0	0.0 ± 0.0	0.0 ± 0.0
Benzo[a]pyrene	0.0 ± 0.0	0.0 ± 0.0	0.0 ± 0.0	0.0 ± 0.0	0.0 ± 0.0	0.0 ± 0.0	0.0 ± 0.0	0.0 ± 0.0
Indeno[1,2,3-cd]pyrene	0.0 ± 0.0	0.0 ± 0.0	0.0 ± 0.0	0.0 ± 0.0	0.0 ± 0.0	0.0 ± 0.0	0.0 ± 0.0	0.0 ± 0.0
Dibenz[a,h]anthracene	0.0 ± 0.0	0.0 ± 0.0	0.0 ± 0.0	0.0 ± 0.0	0.0 ± 0.0	0.0 ± 0.0	0.0 ± 0.0	0.0 ± 0.0
Benzo[ghi]perylene	0.0 ± 0.0	0.0 ± 0.0	0.0 ± 0.0	0.0 ± 0.0	0.0 ± 0.0	0.0 ± 0.0	0.0 ± 0.0	0.0 ± 0.0

Table 9. Concentration of PAHs in surface water at 8 bay sites (December 2022). Unit: ppb or ng/mL. Error bars represent the standard deviation of duplicate samples.

PAHs (ppb)	Site 1	Site 2	Site 3	Site 4	Site 5	Site 6	Site 7	Site 8
Naphthalene	0.2 ± 0.0	0.3 ± 0.0	0.2 ± 0.0	0.2 ± 0.0	0.3 ± 0.0	0.2 ± 0.0	0.3 ± 0.0	0.3 ± 0.0
Acenaphthylene	0.4 ± 0.0	0.0 ± 0.0	0.0 ± 0.0	0.0 ± 0.0	0.0 ± 0.0	0.0 ± 0.0	0.0 ± 0.0	0.0 ± 0.0
Acenaphthene	0.0 ± 0.0	0.0 ± 0.0	0.0 ± 0.0	0.0 ± 0.0	0.0 ± 0.0	0.0 ± 0.0	0.0 ± 0.0	0.0 ± 0.0
Fluorene	0.0 ± 0.0	0.0 ± 0.0	0.0 ± 0.0	0.0 ± 0.0	0.0 ± 0.0	0.0 ± 0.0	0.0 ± 0.0	0.0 ± 0.0
Phenanthrene	1.2 ± 0.0	0.9 ± 0.0	1.2 ± 0.0	1.1 ± 0.0	1.1 ± 0.0	1.2 ± 0.0	1.1 ± 0.0	1.0 ± 0.0
Anthracene	0.6 ± 0.0	0.8 ± 0.0	0.6 ± 0.0	0.6 ± 0.0	0.7 ± 0.0	0.6 ± 0.0	0.6 ± 0.0	0.3 ± 0.3
Fluoranthene	0.7 ± 0.0	0.9 ± 0.0	0.6 ± 0.0	0.3 ± 0.3	0.4 ± 0.4	0.6 ± 0.0	0.7 ± 0.0	0.0 ± 0.0
Pyrene	0.7 ± 0.0	1.0 ± 0.0	0.7 ± 0.0	0.7 ± 0.0	0.8 ± 0.0	0.7 ± 0.0	0.0 ± 0.0	0.0 ± 0.0
Benz[a]anthracene	0.7 ± 0.0	1.0 ± 0.0	0.7 ± 0.0	0.8 ± 0.0	0.8 ± 0.0	0.7 ± 0.0	0.4 ± 0.4	0.0 ± 0.0
Chrysene	1.4 ± 0.1	1.8 ± 0.0	1.1 ± 0.0	1.1 ± 0.0	1.2 ± 0.0	1.0 ± 0.0	1.1 ± 0.0	1.1 ± 0.0
Benzo[b]fluoranthene	1.4 ± 0.1	1.7 ± 0.0	1.1 ± 0.0	1.1 ± 0.0	1.2 ± 0.0	1.1 ± 0.0	1.1 ± 0.0	1.2 ± 0.0
Benzo[k]fluoranthene	1.5 ± 0.0	2.1 ± 0.0	1.3 ± 0.0	1.3 ± 0.0	1.4 ± 0.0	1.1 ± 0.0	1.1 ± 0.0	1.2 ± 0.0
Benzo[a]pyrene	1.5 ± 0.0	2.4 ± 0.0	1.5 ± 0.1	1.4 ± 0.0	1.4 ± 0.0	1.2 ± 0.0	1.2 ± 0.0	1.3 ± 0.0
Indeno[1,2,3-cd]pyrene	1.6 ± 0.0	2.3 ± 0.0	1.4 ± 0.1	1.4 ± 0.0	1.4 ± 0.1	1.2 ± 0.0	1.2 ± 0.0	1.3 ± 0.0
Dibenz[a,h]anthracene	1.4 ± 0.1	2.4 ± 0.2	1.6 ± 0.1	1.5 ± 0.2	1.9 ± 0.0	1.5 ± 0.0	1.2 ± 0.1	1.6 ± 0.0
Benzo[ghi]perylene	1.7 ± 0.1	2.7 ± 0.4	1.7 ± 0.3	2.2 ± 0.0	2.9 ± 0.2	1.6 ± 0.0	1.3 ± 0.0	2.0 ± 0.5